Protocadherin-dependent dendritic self-avoidance regulates neural connectivity and circuit function

Dimitar Kostadinov, Joshua R Sanes

DOI: http://dx.doi.org/10.7554/eLife.08964

Cite as: eLife 2015;10.7554/eLife.08964

Received: 24 May 2015
Accepted: 2 July 2015
Published: 3 July 2015

PROTOCADHERIN-DEPENDENT DENDRITIC SELF-AVOIDANCE REGULATES NEURAL CONNECTIVITY AND CIRCUIT FUNCTION

Dimitar Kostadinov[1,2] and Joshua R. Sanes[1]

[1]Center for Brain Science, Department of Molecular and Cellular Biology, Harvard University, Cambridge, MA 02138

[2]Program in Neuroscience, Harvard Medical School, Boston, MA 02115

Correspondence:
Joshua R. Sanes
Center for Brain Science
Harvard University
52 Oxford Street
Cambridge, MA 02138
sanesj@mcb.harvard.edu

ABSTRACT

Dendritic and axonal arbors of many neuronal types exhibit self-avoidance, in which branches repel each other. In some cases, these neurites interact with those of neighboring neurons, a phenomenon called self/non-self discrimination. The functional roles of these processes remain unknown. Here, we used retinal starburst amacrine cells (SACs), critical components of a direction-selective circuit, to address this issue. In SACs, both processes are mediated by the gamma-protocadherins (Pcdhgs), a family of 22 recognition molecules. We manipulated Pcdhg expression in SACs and recorded from them and their targets, direction-selective ganglion cells (DSGCs). SACs form autapses when self-avoidance is disrupted and fail to form connections with other SACs when self/non-self discrimination is perturbed. Pcdhgs are also required to prune connections between closely spaced SACs. These alterations degrade the direction selectivity of DSGCs. Thus, self-avoidance, self/non-self discrimination, and synapse elimination are essential for proper function of a circuit that computes directional motion.

INTRODUCTION

The geometry of a neuron's dendritic and axonal arbors is believed to be a major determinant of the neuron's role within a circuit. In some cases, the relationship is clear: in sensory systems, for example, the size and shape of a dendritic arbor determines the size and shape of the neuron's receptive field, and the degree of branching within the arbor determines how densely the field is sampled (Lefebvre et al., 2015). Other cases are more conjectural, and in very few cases have experiments attempted to make a causal link between particular dendritic geometries and neuronal function. Here, we address this issue by analyzing a retinal direction-selective circuit.

The phenomena we investigate are self-avoidance and self/non-self discrimination (S/NSD). In self-avoidance, sibling dendritic branches do not contact each other. Although not all neurons exhibit self-avoidance, this phenomenon has been observed in a variety of systems including sensory neurons of leech (in which the process was first described), Manduca sexta, Drosophila, C.elegans, and zebrafish (Grueber et al., 2001; Grueber et al., 2003; Kramer and Kuwada, 1983; Kramer and Stent, 1985; Liu and Halloran, 2005; Nicholls and Baylor, 1968; Sagasti et al., 2005; Smith et al., 2012; Yau, 1976). Dendrites of olfactory projection neurons and axons of mushroom body neurons also exhibit self-avoidance in Drosophila (Hattori et al., 2007; Wang et al., 2002a; Zhan et al., 2004). In mammals, self-avoidance has been documented in cerebellar Purkinje cells and some types of retinal horizontal, bipolar, amacrine and ganglion cells (Lefebvre et al., 2012; Matsuoka et al., 2012; Montague and Friedlander, 1991; Wassle et al., 2009). Several cell-surface proteins have been implicated in self-avoidance, including Dscam1, Turtle, Flamingo, LAR-like receptor tyrosine phosphatase, Unc-5, Unc-6 (Netrin) and Unc-40 (DCC) in invertebrates (Baker and Macagno, 2000; Gao et al., 2000; Long et al., 2009; Matthews et al., 2007; Smith et al., 2012) and Dscam, DscamL1, Slit, Robo, Sema6A, PlexA4, PlexA2, and gamma-Protocadherins (Pcdhgs) in mice (Fuerst et al., 2009;

Fuerst et al., 2008; Gibson et al., 2014; Lefebvre et al., 2012; Matsuoka et al., 2012; Sun et al., 2013). In each case, they appear to act through contact-dependent repellent mechanisms.

In some instances, processes of neurons that exhibit self-avoidance do not avoid other neurons of the same type; rather, they overlap extensively with and sometimes even form synapses on each other. Thus, these neurons appear to discriminate between their own processes, which they repel, and those of their neighbors, with which they interact (**Figure 1A**). This puzzling observation suggests that processes of nominally identical neurons are immune to the repellent forces that act within each other's arbors, a phenomenon that has been called self/non-self discrimination (S/NSD) (Zipursky and Grueber, 2013). Of the molecules that mediate self-avoidance, two have also been shown to mediate S/NSD: fly Dscam1 and mouse Pcdhgs (Hattori et al., 2007; Hughes et al., 2007; Lefebvre et al., 2012; Matthews et al., 2007; Soba et al., 2007). While Dscam1 and Pcdhg proteins are not structurally related, they have three properties that allow them to mediate both self-avoidance and S/NSD. First, both are transmembrane recognition molecules with remarkable extracellular diversity. Alternative splicing of the Dscam1 transcripts and alternative promoter choice (**Figure 1B**) plus isoform multimerization of Pcdhgs lead to >10,000 recognition units (Murata et al., 2004; Schmucker et al., 2000; Schreiner and Weiner, 2010; Tasic et al., 2002; Thu et al., 2014). Second, each Dscam1 and Pcdhg isoform binds homophilically, but does not bind appreciably to other, closely related isoforms (Schreiner and Weiner, 2010; Thu et al., 2014; Wojtowicz et al., 2004; Wojtowicz et al., 2007). Finally, in those cases where tests have been made, each neuron in a population expresses a small randomly selected subset of isoforms (Kaneko et al., 2006; Miura et al., 2013; Neves et al., 2004; Toyoda et al., 2014; Zhan et al., 2004), leading to molecular diversification that, in the case of Drosophila Dscam1, has been demonstrated to be important for proper patterning of neural circuits (Hattori et al., 2009). Together, these observations have led to a model for self-avoidance and S/NSD in which Dscam1- and Pcdhg-mediated homophilic

interactions generate signals leading to repulsion. Because all dendrites (or axons) of a single neuron display the same set of Dscam1 or Pcdhg isoforms, they exhibit self-avoidance. On the other hand, any individual neuron is unlikely to encounter a neighbor that displays the same combination of isoforms, so the neurons do not repel each other, and thus display S/NSD.

These morphological and molecular analyses of self-avoidance and S/NSD have led to several hypotheses about roles they might play in the function of neurons and neuronal circuits. To our knowledge, however, none of these hypotheses has been tested experimentally. Here, we report such tests, focusing on retinal starburst amacrine cells (SACs; **Figure 1C**). These neurons have planar, radially symmetric dendritic arbors that exhibit striking self-avoidance (**Figures 1D**), but they fasciculate and form synapses with neighboring SACs (Lee and Zhou, 2006), and thus exhibit S/NSD. SACs also provide the principal inhibitory input to ON and ON-OFF direction-selective retinal ganglion cells (DSGCs) and are essential for their direction selectivity (Yoshida et al., 2001). Elegant structural and functional studies have revealed the principal elements of the underlying mechanism: individual SAC dendrites are inhibitory direction-selective subunits that wire asymmetrically to DSGCs and inhibit these ganglion cells when visual motion is presented along their proximo-distal axis (Briggman et al., 2011; Euler et al., 2002; Fried et al., 2002; Vaney et al., 2012). Thus, the preferred direction of motion for the DSGC is opposite the preferred direction of motion for the SAC dendrites that innervate it (**Figure 1E**). In addition, SACs form inhibitory synapses onto each other, and it has been suggested that these connections sharpen the directional preference of SAC dendrites and thus the directional preference of the DSGCs that they innervate (Enciso et al., 2010; Lee and Zhou, 2006; Taylor and Smith, 2012).

We showed recently that Pcdhgs mediate self-avoidance and S/NSD in SACs (Lefebvre et al., 2012). Pcdhg-deficient SACs exhibit a dramatic loss of self-avoidance but maintain overlap with

neighboring SACs, as if they mistake their own dendrites for those of their neighbors and fail to repel them. In contrast, forcing all SACs to express the same single Pcdhg isoform restores self-avoidance to individual cells but decreases the overlap between neighboring cells, as if they mistake dendrites of these neighbors for their own and repel them (**Figures 1F-1H**). These results lead to three specific hypotheses about circuit function: (1) in the absence of self-avoidance, SACs will form synapses with themselves (autapses), (2) when S/NSD fails, SACs will form few synapses with each other, and (3) loss of self-avoidance or S/NSD will degrade the direction selectivity of DSGCs. Here, we present evidence in support of these hypotheses, thereby providing insights into the functional roles of self-avoidance and S/NSD. We also demonstrate an unexpected role of Pcdhgs in control of synapse elimination.

RESULTS

SACs are connected by inhibitory synapses

Zheng et al. (2004) demonstrated the presence of GABAergic synapses between SACs shortly after eye-opening in rabbits. To begin this study, we confirmed that similar connections occur in young mice and asked whether they persist in adults. In addition to releasing GABA, SACs also release acetylcholine, the only retinal neuron to do so (Famiglietti, 1983; Hayden et al., 1980), so we used a line that expresses Cre recombinase from the choline acetyltransferase locus to mark and manipulate them selectively ($Chat^{cre}$; Rossi et al., 2011). We mated $Chat^{cre}$ mice to lines that express Cre-dependent fluorescent reporters (Buffelli et al., 2003; Madisen et al., 2010), identified SACs in explants, and recorded from pairs of ON SACs shortly after eye opening (postnatal day [P] 15-24; eye opening occurs at P14) and in young adults (P40-100) (**Figure 2A**). We refer to wild-type SACs as $Pcdhg^{22}$ SACs, since they have their full complement of Pcdhgs. In each case, we tested pairs separated by distances varying from 35 to 175μm; the dendritic radius of SACs in living tissue is ~100μm, and varies little between P15 and P100 (**Figure 2 – figure supplement 1A-B**). For each pair, we stepped presynaptic SACs

from a holding potential (V_h) of -70 mV to +20 mV while holding postsynaptic SACs at +30 mV to record inhibitory currents. In the majority of cases, we obtained bidirectional recordings; we found fewer unidirectional connections between neighboring pairs than would be expected by chance (**Figure 2 – figure supplement 2D**).

Stimulation of a SAC elicited an inhibitory current in a neighboring SAC in some but not all pairs tested at P15-24 and P40-100 (**Figures 2B-2C**). Currents occurred with a latency of ~7ms and averaged ~15 pA in connected cells at both ages (**Figure 2J**). They were blocked by 50 μM picrotoxin and reversed at the chloride reversal potential for our recording solutions (~-70 mV), indicating that they were GABAergic and inhibitory (**Figure 2 – figure supplement 2A-C**). Although SAC-SAC connections have a cholinergic component before eye-opening in both rabbits and mice (Ford et al., 2012; Zheng et al., 2004), they exhibited no significant cholinergic component after eye opening (data not shown).

Synapses between closely spaced SACs are eliminated after eye-opening

The frequency with which SACs were interconnected varied systematically with the distance between their somata and with age. At P15-24, pairs were over twice as likely to be connected if they were separated by 35-100μm than if they were separated by 100-175μm (**Figure 2F and 2K, left**). This difference mirrors the inverse relationship of the distance between SACs and the overlap of their dendritic arbors (**Figure 2 – figure supplement 1C**). In contrast, connections were seldom detectable between pairs separated by <100μm in adults. The frequency of connections between pairs >100μm apart did not change significantly with age (**Figures 2G and 2K, right**), indicating that the decline did not reflect decreased ability to detect connections in older mice. The most parsimonious explanation for this difference is that synapses between closely-spaced SACs are eliminated as SACs mature.

Pcdhgs drive elimination of connections between closely spaced SACs

Next, we asked whether Pcdhgs are required for formation of SAC-SAC synapses. For this purpose, we inactivated all 22 Pcdhgs in SACs using a conditional Pcdhg allele ($Pcdhg^{flox}$) (Lefebvre et al., 2008) and the $Chat^{cre}$ line. We refer to $Pcdhg^{flox/flox}$;$Chat^{cre}$ mice as $Pcdhg^{0}$ and controls ($Pcdhg^{flox/+}$ or $Pcdhg^{+/+}$; $Chat^{cre}$) as $Pcdhg^{22}$. Restricting mutation to SACs allowed us to analyze roles of Pcdhgs in SACs without the complication of directly affecting other synaptic partners. Moreover, deletion of Pcdhgs leads to excessive cell death in many retinal neuronal populations, but not in SACs (Lefebvre et al., 2012; Lefebvre et al., 2008). As expected, we observed no alterations in the density of SACs or of other retinal cells in $Pcdhg^{0}$ retinas. We further verified that the laminar position and mosaic spacing of SACs, as well as overall retinal structure, did not differ detectably between $Pcdhg^{22}$ and $Pcdhg^{0}$ retinas (**Figure 2 – figure supplements 3 and 4**).

At P15-24, the number and strength of SAC-SAC connections were similar in $Pcdhg^{22}$ and $Pcdhg^{0}$ retinas: in both genotypes, connections were over twice as common in closely spaced pairs than in pairs separated by >100μm and current sizes did not differ significantly between $Pcdhg^{22}$ and $Pcdhg^{0}$ retinas (**Figures 2D, 2H, and 2J**). Thus, Pcdhgs are dispensable for formation of SAC-SAC synapses. In adults, in contrast, the pattern of SAC-SAC connectivity differed between $Pcdhg^{22}$ and $Pcdhg^{0}$ mice. Synapses between closely spaced SACs were retained in mutants during the period that they were lost from controls (**Figures 2E, 2G, 2I, and 2K**). This loss of proximal connections was selective in that the frequency and size of connections between SACs separated by >100μm did not differ significantly between $Pcdhg^{22}$ and $Pcdhg^{0}$ mice (**Figures 2J-2K)**. These results reveal a requirement of Pcdhgs for synapse elimination.

Pcdhgs prevent formation of SAC autapses

If $Pcdhg^{0}$ SAC dendrites treat other dendrites of the same SAC as if they are dendrites of other SACs, we wondered whether they would form autapses. To test this hypothesis, we adapted a protocol that had been used to elicit autaptic currents in cultured neurons and cortical slices (Bacci et al., 2003; Bekkers and Stevens, 1991). We stimulated SACs with brief voltage steps to very positive potentials (V = +60 mV, 2-4 ms), then returned to more negative potentials (V = -20 mV) (**Figure 3A**). We confirmed that this stimulation was able to elicit synaptic release in paired recordings (**Figure 3 – figure supplement 1A**). These stimuli elicited autaptic currents in ~75% of $Pcdhg^{0}$ SACs at P21-24, but in no $Pcdhg^{22}$ SACs (**Figures 3B and 3C**). Autaptic currents resembled SAC-SAC connections in their latencies and rise times, were blockable by application of 50 μM Picrotoxin, and averaged ~20pA in size (**Figures 3F-3G and Figure 3 – figure supplement 1B-C**). We also asked whether autapses are present in adult $Pcdhg^{0}$ SACs or whether, like synapses between closely-spaced SACs in wild-type retina (see previous section), they are progressively eliminated. Autapses persisted into adulthood in $Pcdhg^{0}$ SACs with sizes and frequency similar to those observed at P21-24 (**Figures 3D-3G**). Thus, one role of Pcdhg-mediated self-avoidance is to prevent formation of autapses.

SACs that express the same Pcdhg isoform are seldom connected to each other

The proposed mechanism for Pcdhg-dependent S/NSD is that the stochastic expression of a subset of Pcdhg isoforms endows each SAC with a unique molecular identity that circumvents Pcdhg-dependent avoidance, allowing neighboring SACs to interact (Lefebvre et al., 2012). We hypothesized that if all SACs expressed the same Pcdhg isoform, they would treat dendrites of other SACs as if they were other dendrites of the same SAC, and form few SAC-SAC synapses. To test this idea, we used a mouse line in which a single Pcdhg isoform (PcdhgC3) can be expressed in any cell type in a Cre-dependent manner (Lefebvre et al., 2012). We call mice in which SACs expressed only this isoform $Pcdhg^{1}$ (Rosa-CAGS-lox-stop-lox-PcdhgC3-mCherry;$Chat^{cre}$;$Pcdhg^{flox/flox}$).

The overall morphology, number, and spacing of SACs, as well as overall retina structure, were normal in Pcdhg^{1} mice (**Figure 4A and Figure 2 – figure supplements 3 and 4**), and SAC dendrites formed a fine plexus within which, despite a decrease in overlap between pairs of neurons (Lefebvre et al., 2012), they had ample opportunity to come into close proximity to each other (**Figure 4B**). We made paired recordings from SACs in Pcdhg^{1} mice at P15-24 using methods described in Figure 2 (**Figures 4C-4D**). The frequency of SAC-SAC connections in Pcdhg^{1} mice was ~20% of that in Pcdhg^{22} or Pcdhg^{0} mice (**Figure 4F**). Similarly, currents in connected pairs were in Pcdhg^{1} mice averaged ~40% of that in Pcdhg^{22} or Pcdhg^{0} mice (**Figure 4H**). Thus, forcing expression of the same Pcdhg isoform in all SACs decreased their connection strength to <10% (0.2 x 0.4) of controls. A similar decrease was observed in adult Pcdhg^{1} retinas (**Figure 4E, 4G-4H**). We conclude that Pcdhg diversity is required for functional connectivity between neighboring SACs.

Pcdhgs are dispensable for connections of SACs with bipolar and ganglion cells

Having found that manipulation of Pcdhg expression affects the ability of SACs to form synapses on their own dendrites or those of other SACs, we asked whether such manipulations affect their ability to receive synapses from bipolar cells or form synapses onto DSGCs. We used visual stimuli based on previous findings that the main visually-evoked excitatory input to SACs is from bipolar cells, and that SACs provide the main inhibitory input to DSGCs (**Figure 5A**) (Helmstaedter et al., 2013; Hoggarth et al., 2015; Taylor and Wassle, 1995; Vaney et al., 2012).

To assess bipolar input to SACs, we recorded from ON SACs while holding the cells at V_h = -70 mV and presenting bright spot flashes centered on the soma of the recorded cell. SACs

received strong excitatory inputs in Pcdhg^{22}, Pcdhg^{0} and Pcdhg^{1} mice, with no significant differences among them (**Figures 5B-5C**).

Four populations of ON-OFF DSGCs have been described, each tuned to one of the cardinal directions: dorsal, ventral, nasal and temporal (Barlow and Hill, 1963; Elstrott et al., 2008; Oyster and Barlow, 1967). Their physiological properties other than preferred direction are similar, but they exhibit molecular differences that allow them to be marked selectively (Kay et al., 2011). To assess SAC input to DSGCs, we used a transgenic line in which DSGCs that prefer motion in the ventral direction express GFP (HB9-GFP; Trenholm et al., 2011). We introduced this transgene into the Pcdhg^{22}, Pcdhg^{0} and Pcdhg^{1} backgrounds, and recorded inhibitory currents (V_h= 0 mV) from GFP-labeled DSGCs, which we call vDSGCs here. Sizes of both ON and OFF inhibitory responses to spot flashes were indistinguishable across the three genotypes (**Figures 5D-5E**). Similarly, excitatory spot flash responses in vDSGCs were unaffected by manipulation of Pcdhgs in SACs (**Figures 5F-5G**). Thus, Pcdhg expression in SACs is dispensable for their ability to form and maintain synapses with other cell types.

We also assessed the structure of vDSGCs in Pcdhg^{22}, Pcdhg^{0}, and Pcdhg^{1} mice. We filled single cells with fluorescent dye, stained SACs with antibodies to ChAT, and imaged the two cell types. In all conditions, the ON and OFF dendrites of these DSGCs stratified in the ON and OFF SAC plexus, fasciculated with SAC dendrites, and maintained their modest structural asymmetry (**Figures 5H-5J**). Thus, altering Pcdhg expression in SACs had no detectable effect on the morphology of vDSGCs. We also validated that altering Pcdhg expression in SACs did not affect cell number, mosaic spacing, or expression patterns of vDSGCs (**Figure 5 – figure supplement 1**).

Loss of SAC self-avoidance or S/NSD degrades direction selectivity of DSGCs

We next tested the hypothesis that loss of self-avoidance or S/NSD degrades the information-processing ability of SACs within the direction-selective circuit. To this end, we recorded spikes from vDSGCs while moving a bright bar over their receptive field in 8 different directions. Because vDSGCs are all tuned to a single direction in wild-type mice, we were able to ask whether manipulation of Pcdhgs affects preferred direction as well as the degree of direction selectivity.

vDSGCs in $Pcdhg^{22}$ mice exhibited strong ON and OFF directional responses (**Figures 6A**) as shown previously (Duan et al., 2014; Kim et al., 2010; Trenholm et al., 2011). We calculated a direction-selective index (DSI) for each vDSGC by computing the vector sum of the responses to different directions (Kim et al., 2008) and calculated both the magnitude of directional responses and the angle of preference (**Figure 6B**). Direction selectivity of vDSGCs was diminished in both $Pcdhg^{0}$ and $Pcdhg^{1}$ retinas, but in different ways. In both genotypes, the magnitude of the DSI vectors was significantly decreased with respect to controls (by ~50% in $Pcdhg^{0}$ and ~35% in $Pcdhg^{1}$; **Figures 6C-6G**). In contrast, responses of vDSGCs in $Pcdhg^{0}$ retinas exhibited a significantly greater scatter around the ventral axis than those in wild-type retinas, whereas vDSGCs in $Pcdhg^{1}$ retinas were as precisely tuned to ventral motion as controls (**Figures 6C-6F, 6H and Figure 6 – figure supplement 1**). This variance likely reflects the contorted morphology of SAC dendrites in $Pcdhg^{0}$ but not $Pcdhg^{1}$ retinas. Likewise, the variation between the preferred direction of ON and OFF responses was greater in $Pcdhg^{0}$ retinas than in either $Pcdhg^{22}$ or $Pcdhg^{1}$ retinas, indicating that SAC morphology and connectivity are disrupted independently in the ON and OFF SAC layers (**Figure 6I**).

To obtain a single measure of how well vDSGCs reported on ventral motion, we projected the directional vectors onto the ventral axis. This gave us a ventral DSI that combined the degree of directional preference and the fidelity of ventral preference for ON and OFF responses together.

vDSGCs in Pcdhg^{22} (control) retinas were most ventrally selective, followed by those in Pcdhg^{1} retinas; vDSGCs in Pcdhg^{0} retinas were the least selective (**Figure 6J**). Together, these results demonstrate that manipulating Pcdhg expression in SACs, and thereby attenuating self-avoidance or S/NSD, degrades the direction selectivity of DSGCs. Recently, Sun et al., (2013) also showed that morphological alterations of SACs disrupt directional tuning of DSGCs.

Previous studies have shown that direction-selective responses are already present at eye opening in mice but become more selective with age (Chan and Chiao, 2013; Chen et al., 2014; Elstrott et al., 2008; Yonehara et al., 2011). We wondered whether this improvement of direction selectivity with age was related to the loss of proximal SAC-SAC connections. To assess this possibility, we recorded from direction-selective responses from vDSGCs at P15-24 in Pcdhg^{0} mice, which do not go through a developmental change in SAC-SAC connectivity. We confirmed the improved age-dependent directional tuning of DSGCs in control retinas. In contrast, direction selectivity of vDSGCs did not improve in Pcdhg^{0} retinas (**Figure 6 – figure supplement 2**). This result is consistent the idea that developmental refinement in SAC-SAC connectivity contributes to age-dependent improvement in direction selectivity.

Synaptic mechanisms underlying effects of Pcdhgs on direction selectivity

Finally, we sought to explain the degradation of directional selectivity of vDSGCs in Pcdhg^{0}, and Pcdhg^{1} retinas (**Figure 6**) in terms of alterations in SAC connectivity (**Figures 2-4**). To this end, we recorded inhibitory and excitatory currents from vDSGCs in the three genotypes in response to bars moving in the null and preferred directions (dorsal and ventral, respectively). As noted previously, the inhibitory currents arise predominantly from SACs, which are genetically altered in mutants, while the excitatory currents arise predominantly from bipolar cells, which are not altered.

Studies in mice and rabbits have revealed two key aspects of SAC-DSGC connectivity that lead to direction selectivity (Fried et al., 2002; Park et al., 2014; Taylor and Vaney, 2002; Vaney et al., 2012; Yonehara et al., 2013), both of which we confirmed in vDSGCs from $Pcdhg^{22}$ retinas. First, inhibitory input to DSGCs is greater for movement in the null direction (dorsal for vDSGCs) than for movement in the preferred direction (ventral for vDSGCs), whereas excitatory input is similar for movement in both directions (**Figures 7A, 7J, and 7K**). Second, excitatory and inhibitory currents recorded from DSGCs arise at the same time when motion is in the null direction, whereas inhibitory currents lag with respect to excitatory currents when motion is in the preferred direction (**Figures 7B, 7L, and 7M**). Together, these features allow inhibition to veto excitation in DSGCs more strongly for null motion than for preferred motion. Consequently, net depolarization in DSGCs is largest for motion in the preferred direction.

We found that both of these contributors to direction selectivity were blunted in $Pcdhg^{0}$ and $Pcdhg^{1}$ retinas (**Figures 7D-7E, 7G-7H and Figure 6 – figure supplement 1**). First, inhibitory currents were larger for ventral motion and smaller for dorsal motion in $Pcdhg^{0}$ and $Pcdhg^{1}$ retinas than in $Pcdhg^{22}$ retinas, with no significant change in excitation **(Figures 7J-7K**). The difference from control values was greater for $Pcdhg^{0}$ than for $Pcdhg^{1}$ retinas but significant in both. Second, the delay of inhibition in response to preferred motion was less in $Pcdhg^{0}$ and $Pcdhg^{1}$ retinas than in $Pcdhg^{22}$ retinas, with no significant change for movement in the null direction; in this case, $Pcdhg^{0}$ and $Pcdhg^{1}$ retinas were equally affected (**Figures 7L-7M**). Thus, the ability of inhibition to veto excitation for preferred motion was greater in $Pcdhg^{0}$ and $Pcdhg^{1}$ retinas than in $Pcdhg^{22}$ retinas. It is likely that the differences in the size and timing of inhibitory currents in vDSGCs from $Pcdhg^{0}$ and $Pcdhg^{1}$ retinas result in the changes in spiking observed in Figure 6. In the Discussion, we suggest a possible explanation for these alterations in terms of perturbations in SAC self-avoidance, S/NSD, and synapse elimination.

DISCUSSION

Dendritic arbors of many neuronal types in both vertebrates and invertebrates exhibit self-avoidance and S/NSD (references in Introduction). In this study, we used SACs to assess the functional consequences of perturbing these processes. SACs were uniquely suited for this study for several reasons. First, they exhibit robust self-avoidance and S/NSD. Second, Pcdhgs are necessary for both processes, providing a means to manipulate them. Moreover, our genetic methods allowed us to manipulate Pcdhgs selectively in SACs, without directly affecting other neuronal types to which they connect. Third, removal or replacement of Pcdhgs in SACs allowed us to perturb self-avoidance and S/NSD independently. Finally, the role of SACs in retinal circuit function is remarkably well understood. By exploiting these features, we elucidated roles of self-avoidance and S/NSD in SAC connectivity, discovered a previously undescribed phase of synapse elimination between SACs, and showed that alterations in these processes decrease the ability of the retina to compute direction of motion.

Linking Pcdhg expression to SAC connectivity

Loss of Pcdhgs has been shown to have several effects on developing neurons including decreased neuronal survival in retina and spinal cord, decreased synaptic maintenance in spinal cord, decreased dendritic branching in neocortex, and decreased self-avoidance in retina and cerebellum (Garrett et al., 2012; Lefebvre et al., 2012; Lefebvre et al., 2008; Prasad et al., 2008; Wang et al., 2002b; Weiner et al., 2005). Any of these phenotypes would complicate our attempt to assess roles of self-avoidance and S/NSD in SAC and circuit function. We therefore manipulated Pcdhg expression selectively in SACs and performed a variety of control experiments to assess whether our manipulations affected other aspects of retinal development or function. Our results are as follows:

First, SACs are unusual among retinal neurons in that their survival does not depend on Pcdhg expression (Lefebvre et al., 2012), and we confirmed that SAC number was unaltered in $Pcdhg^{0}$ and $Pcdhg^{1}$ retina. Second, we confirmed (Lefebvre et al., 2012) that alteration of Pcdhg expression in SACs had no effect on their dendritic length or mosaic spacing. Third, basic electrical properties (resting membrane potential and input resistance) of SACs were preserved in $Pcdhg^{0}$ and $Pcdhg^{1}$ retinas (data not shown). Fourth, manipulation of Pcdhgs in SACs had no detectable effect on the strength of the inputs they receive from bipolar cells or deliver to DSGCs. Fifth, removing or replacing Pcdhgs in SACs had no detectable effect on cell number or general organization of the retina. Finally, we detected no alteration in the number, spacing, dendritic arbors, molecular markers or electrical properties of a subset of ventrally-preferring DSGCs. Thus, although we cannot completely exclude the possibility that Pcdhg manipulation had additional effect, we favor the explanation that alterations in SAC connectivity and circuit function documented here result from perturbation of Pcdhg-dependent self-avoidance, S/NSD and synapse elimination.

Self-avoidance, self/non-self discrimination and SAC connectivity

Morphological studies led to the idea that self-avoidance serves to optimize coverage of a receptive field by a dendritic arbor, minimizing gaps and clumps (Grueber and Sagasti, 2010; Kramer and Kuwada, 1983; Kramer and Stent, 1985). Our physiological studies revealed an additional role of self-avoidance in SACs: it prevents formation of autapses (**Figure 3**). In many neuronal types, autapses cannot form because pre- and postsynaptic machinery are confined to axons and dendrites, respectively, which are physically segregated. SACs, in contrast, form dendro-dendritic synapses, and therefore have pre- and postsynaptic specializations intermingled. This situation is not uncommon in the retina and elsewhere in the central nervous system, such as the olfactory bulb (Murthy, 2011). We suggest that self-avoidance may play similar roles in other such cells.

S/NSD is generally viewed as a means of limiting inter-dendritic repulsion to sibling processes, so that neurons of a single type can share territory (Grueber and Sagasti, 2010; Lefebvre et al., 2015; Zipursky and Grueber, 2013). In the retina, it additionally allows formation of synapses between SACs. Several types of neurons have been shown to form homotypic connections in cortex and cerebellum (Pfeffer et al., 2013; Rieubland et al., 2014). Since most molecules described to date that mediate self-avoidance are ill-suited to mediate S/NSD, additional mechanisms likely remain to be discovered. In addition, some cell types that connect homotypically may lack robust mechanisms for self-avoidance. Indeed, cortical fast-spiking interneurons, which form homotypic connections, also form autapses (Bacci et al., 2003). It is unclear whether these autapses are beneficial to the circuit or whether they are an acceptable cost of homotypic connectivity.

Age- and distance-dependent elimination of SAC-SAC connections

Zhou and colleagues previously demonstrated inhibitory SAC-SAC synaptic connections in rabbit retina soon after eye opening, a result we confirmed here for mouse (Lee and Zhou, 2006; Zheng et al., 2004). We also discovered two additional features of these connections. First, in mature retina (>P40), SACs separated by less that 100μm seldom formed synapses with each other, whereas SACs separated by >100μm were connected frequently. Since dendritic overlap is inversely proportional to the distance between SACs, this distance-dependence is not a passive consequence of proximity but instead implies spatial selectivity to SAC-SAC connections. Second, we found that this distance-dependence was absent in immature retinas (P15-24; eye opening occurs at P14). Thus, connections between closely-spaced SACs are selectively eliminated as the retina matures.

We view the loss of proximal SAC-SAC connections as synapse elimination, a process that occurs in many and perhaps most neuronal types (Kano and Hashimoto, 2009), but has not previously been described for SACs. In most cases, synapse elimination was first described physiologically (Crepel et al., 1976; Purves and Lichtman, 1980; Redfern, 1970) as we have done here. For these cases, morphological confirmation was obtained many years later. We expect this will be the case for SACs as well. Such demonstration will be difficult, however, because SAC dendrites are so thin and densely packed that it is infeasible to map synapses on them by light microscopic methods. Ultrastructural studies using genetic tags or extensive reconstruction at several developmental time points will therefore be needed to decide this issue.

Why might connections between closely-spaced SACs be counterproductive? Inhibitory connections between nearby SACs would frequently be made between dendrites with similar directional preferences. The ability of a SAC dendrite to respond to centrifugal motion along its dendrite would thereby decrease, because this motion would lead to inhibition of the dendrite by other SACs. This, in turn, would degrade the direction selectivity of DSGCs (Taylor and Smith, 2012). In contrast, connections of distant SACs will most frequently be made between dendrites with opposite directional preference; as discussed in the next section, this enhances directional computation.

Conversely, might there be a role for connections between closely-spaced SACs early in development? In fact, strong SAC-SAC connectivity is critical for the developing visual system, because it underlies propagation of the retinal waves that pattern the segregation of binocular input in retinorecipient areas such as the superior colliculus and lateral geniculate nucleus (Ackman and Crair, 2014; Burbridge et al., 2014; Ford et al., 2012). Because waves occur before eye-opening, directional selectivity is unimportant. Thus, we suggest that postponing

443 distance-dependent elimination of SAC-SAC connections until after eye-opening allows both the
444 dense connectivity needed for wave propagation and the selective anti-parallel connectivity
445 needed for direction selectivity. Consistent with this view, the direction selectivity of DSGCs
446 increases during the period in which connections between closely-spaced SACs are being
447 eliminated.
448
449 We also found that connections between closely-spaced SACs are not eliminated in the
450 absence of Pcdhgs, revealing a novel role for these molecules in neural development.
451 The mechanism of this effect remains to be determined. One attractive possibility is that an
452 uneven distribution of Pcdhgs within SACs might confine synapses to distal portions of
453 dendrites.
454
455 **Roles of SAC-SAC inhibition in directional computation**
456 We have argued that alterations in SAC connectivity in $Pcdhg^{0}$ and $Pcdhg^{1}$ retinas documented
457 in the first part of this study (**Figures 2-4**) result from defects in self-avoidance, S/NSD and
458 synapse elimination. We now argue that these defects largely explain the degradation in
459 direction selectivity in vDSGCs documented in the second part (**Figures 6-7**).
460
461 As described above, SACs contribute to the direction selectivity of DSCGs in two ways. First,
462 inhibitory currents are larger during null motion than preferred motion. The difference in
463 inhibitory currents arises in large part from the geometric arrangement of SAC-DSGC
464 connections: vDGSCs, for example, receive most SAC input from dendrites that respond
465 preferentially to dorsal (null) motion (Briggman et al., 2011). In addition, anti-parallel inhibitory
466 connections between SACs decrease the currents that these dendrites would otherwise provide
467 during preferred motion (**Figure 7C**). Together, these processes result in greater net
468 depolarization and therefore spiking for preferred motion than null motion. The number of SAC-

SAC connections is markedly decreased in Pcdhg^{1} retinas (**Figure 7I**). These connections persist in Pcdhg^{0} retinas, but their efficacy is decreased because parallel SAC dendrites remain connected and inhibit each other, resulting in decreased inhibitory input from SACs to DSCGs for null motion and decreased antiparallel SAC-SAC inhibition (and thus increased SAC-DSCG inhibition) for preferred motion (**Figure 7F**). The autapses in Pcdhg^{0} retina would act similarly to synapses between parallel dendrites, since autapsing dendrites are likely to point in similar directions (see Pcdhg^{0} SAC image in **Figure 3**).

Second, inhibitory and excitatory currents in DSGCs are nearly simultaneous during null motion, allowing inhibition to veto excitation, whereas inhibition is delayed with respect to excitation during preferred motion, decreasing the power of the veto. A recent computational model argues that the delayed inhibition for preferred motion arises in part because anti-parallel SAC-SAC connections transiently suppress transmitter release from SACs to DSGCs (Taylor and Smith, 2012). Decreased inhibition, from loss of SAC-SAC connections in Pcdhg^{1} retinas and decreased efficacy of SAC-SAC synapses Pcdhg^{0} retinas, would thus be expected to decrease the delay, thereby blunting the response to preferred motion.

In summary, the spatial organization of SAC-SAC inhibition and SAC-DSGC inhibition work together to generate a direction-selective output from the retina. When self-avoidance, S/NSD, or synapse elimination is perturbed, SAC-SAC inhibition is rendered less effective and direction selectivity is degraded. Thus, our results demonstrate roles for these Pcdhg-dependent processes in computation of direction selectivity and provide new evidence in support of the hypothesis (Enciso et al., 2010; Lee and Zhou, 2006; Taylor and Smith, 2012; Vaney et al., 2012) that SAC-SAC connections play important roles in this computation.

MATERIALS AND METHODS

Animals

Animals were used in accordance with NIH guidelines and protocols approved by Institutional Animal Use and Care Committee at Harvard University. All mice were maintained on a C57BL/6 background. The lines used were reported previously: $Pcdhg^{fcon3}$ (Lefebvre et al., 2012; Lefebvre et al., 2008; Prasad et al., 2008), $Chat^{Cre}$ (Rossi et al., 2011), Thy1-stop-YFP line #15 (Buffelli et al., 2003), Mnx1::eGFP (here called HB9-GFP) (Trenholm et al., 2011; Wichterle et al., 2002), RC-stop-tdTomato (Madisen et al., 2010), and RC-stop-PcdhgC3-mCherry (Lefebvre et al., 2012). We generally used $Chat^{Cre}$ mice as homozygotes, because we found that this gave earlier and more even Cre activity at P1, when SAC dendrites are beginning to elaborate.

Electrophysiology

Mice were dark adapted for at least 2 hours prior to euthanasia. Retinas were rapidly dissected under infrared illumination into room temperature, oxygenated (95% O_2, 5% CO_2) Ames medium and placed in a recording chamber on the stage of a custom built electrophysiology set up. Recordings were carried out in same medium heated to 32-34^{o}C. Fluorescent cells were identified with a brief (<40 ms) LED flash, overlaid onto infrared images, and targeted with electrodes. Recordings were made from SACs and vDSGCs using patch electrodes with resistance of 6-8 MΩ and 4-6 MΩ, respectively. For loose patch recordings, electrodes were filled with Ames medium. For intracellular recordings, electrodes were filled with intracellular solution containing the following (in mM): 120 Cs-Methanesulfonate, 10 Na-Acetate, 0.2 $CaCl_2$, 1 $MgCl_2$, 10 EGTA, 5 CsCl, 2 Mg-GTP, and 0.5 Na_2-GTP (pH 7.3). Intracellular recording solutions were supplemented with 5mM QX314-Br for vDSGC voltage clamp recordings and 5mM TEA-Br for SAC autapse recordings.

Paired connections were tested with 200 ms voltage steps from Vh = -70 mV to +20 mV in presynaptic SACs while postsynaptic SACs were held at +30 mV for all current size measurements and at potentials between -70 and +30 in 20 mV increments to establish I-V relationships. Approximately 10 voltage step repetitions were acquired for each pre-post pair and bidirectional measurements were made if recordings were sufficiently stable. Cells were analyzed in a semi-automated fashion and deemed connected using the following criteria: (1) Average traces had a peak in the first 30 ms after presynaptic stimulus onset that was >2 standard deviations from the baseline established in the 50 ms before stimulus onset, (2) current deflection was present in ≥ 80% of trials, (3) Peak current had short latency (<12 ms) and fast rise time (10-90% rise time < 4 ms). Each recording was checked after the fact for large baseline deviations or other anomalous signals.

Autapse recordings were evoked using a brief voltage step from Vh = -70 to +60 mV (2-4 ms) followed by a return to -20 mV. This stimulus activated some intrinsic currents in SAC that decayed in <100 ms. During this decay phase, a large fraction $Pcdhg^{0}$ SACs exhibited outward currents with synaptic latencies, rise times, and amplitudes that were blockable by the addition of 50 μM Picrotoxin and thus autaptic currents. To analyze these recordings, we (1) fit the first 30 ms of each trace after returning to our holding potential of -20 mV with a double exponential curve, (2) looked for residuals of the fit >2 standard deviations of the pre-stimulus baseline in order to identify SACs that potentially made autapses, and (3) applied criteria used to find connected SAC pairs. We could not make reliable measurements of autapses in SACs from retinas younger than P21 due to large inward calcium currents evoked by depolarization. These currents were also apparent at even younger ages (P8), and may therefore be residually present from the ages at which SACs initiate and propagate retinal waves (see Discussion).

In loose patch spike recordings, action potentials were detected and analyzed using a simple thresholding criterion in MATLAB (Mathworks). Spikes histograms were made with 50 ms bins and used to find peak firing rates. Direction-selective indices (DSIs) and preferred directions of individual cells were calculated using the maximal firing rates elicited by moving visual stimuli in 8 directions ($\theta = 0^o:45^o:315^o$) and vector sums were calculated as in Kim et al., 2008.

Visual stimuli

Light stimuli were presented using a modified DLP projector (Dell) suspended underneath the microscope stage with a custom substage lens system focused onto the retinal photoreceptors. Monochrome light was used (wavelength peak = 405 nm) at a background intensity 5×10^2 R*/rod/s set using neutral density filters. Visual stimuli were presented at 100:1 positive contrast and patterns generated using Psychophysics Toolbox in MATLAB (Mathworks) and are available as Source code 1. All stimuli were centered on the cell body of recorded neurons. Spot flash stimuli were 300 μm-diameter circles. Moving bars were 1000-1500 μm long and 300 μm wide, travelled at 1000 μm/s, presented moving along their long axis in 8 directions, and rotated by 135^o with each presentation. At the speeds we used for our visual stimuli, nonlinear dendritic processes contributing to directional tuning are not observed in HB9-GFP vDSGCs (Trenholm et al., 2011). A minimum of 4 repetitions were presented for each stimulus.

Data acquisition and analysis

Electrophysiological recordings were acquired using a Multiclamp 700B Amplifier (Molecular Devices) at 20 kHz. Acquisition was controlled by custom LabView software (National Instruments) and is available as Source code 2. Data were analyzed using custom written MATLAB software (Mathworks) available as Source code 3 and displayed in IgorPro (Wavemetrics). All statistics were calculated in MATLAB. Pairwise comparisons were made using two-tailed t-test, and multiple samples were compared using one-way analysis of variance

(ANOVA). Errors on connection probability were calculated using the variance of the binomial distribution. The specificity of reciprocal connections between neighboring SACs was assessed by comparison with Monte Carlo simulations using recorded connection probabilities.

Latencies for paired recordings from SACs and directional voltage-clamp recordings from vDSGCs were measured by fitting the rising phase of each current using a Boltzmann function in IgorPro (Wavemetrics) and finding the intersection this line with the baseline. Latencies of autaptic currents (after automated detection) were calculated manually and taken from the beginning of the short voltage steps to +60 mV.

SAC and DSGC fills and histology

SACs and DSGCs were filled through patch electrodes using methods described above. Alexa Fluor 488 hydrazide (200 μM) was added to the intracellular recording solution, and recordings were maintained for ~20 minutes in current-clamp mode while maintaining a negative holding potential (<-60mV). After individual cells were filled, retinas were either imaged live (to measure SAC dendritic radius) or immediately placed in fixative and processed for histology.

Mice used exclusively for histology were euthanized by intraperitoneal injection of pentobarbital or euthasol and either enucleated immediately or transcardially perfused with Ringer's solution followed by 4% paraformaldehyde (PFA) in PBS. Eye cups were removed and fixed in 4% PFA in PBS on ice for one hour then rinsed with PBS. Retinas were analyzed as whole mounts or cryosections as described previously (Lefebvre et al., 2012). Whole mount retinas were incubated in blocking buffer (0.5% Triton-X-100, 5% normal donkey serum in PBS) for 1-2 hours at room temperature, then incubated for 5-7 days at 4^{o}C with primary antibodies. For cryosections, fixed retinas were incubated with 30% sucrose/PBS for >2 hours (until they lost buoyancy), frozen, and sectioned at 20 μm in a cryostat. Sections were blocked with 5% donkey

serum/0.5% Triton X-100/PBS for 1-2 hours at room temperature, with primary antibodies overnight at 4^{o}C, and with secondary antibodies for 2 hours at room temperature. Whole mount retinas or sections were mounted onto glass slides using Fluoromount G (Southern Biotech). The following primary antibodies were used: chick anti-GFP (1:500, Abcam); rabbit anti-DsRed (1:1000, Clontech); goat anti-choline acetyltransferase (ChAT) (1:400, Millipore); goat anti-VAChT (1:1000, Promega); rabbit anti-Calbindin (1:2500, Swant); rabbit anti-CART (1:1000, Phoenix); mouse anti-Brn3a (1:1000, Millipore); goat anti-Chx10 (1:200, Santa Cruz); and mouse anti-AP2 (1:1000, DSHB). Nuclei were labeled with TO-PRO3 (1:3000, Invitrogen). Secondary antibodies were conjugated to Alexa Fluor 488, Alexa Fluor 568 (Invitrogen), or DyLight 649 (Jackson ImmunoResearch) and used at 1:1000.

Immunofluorescence samples were imaged using Olympus FV1000 confocal microscope using 488, 568, and 647 lasers with a z-step size of 1.0 µm. FIJI (NIH) was used to analyze confocal stacks and generate maximum intensity projections. ON and OFF dendrites of DSGCs were separated using depths in the IPL and corresponding SAC bands. Retinal orientations were maintained throughout.

AUTHOR CONTRIBUTIONS

D.K. and J.R.S. planned experiments, analyzed data, and wrote the paper. D.K. performed all experiments.

ACKNOWLEDGEMENTS

We thank members of the Sanes lab (official and adopted) for useful discussions and comments on this manuscript, J. Lefebvre for guidance during initial stages of the project and comments on this manuscript, E. Soucy and J. Greenwood for assistance in construction of electrophysiology set-up, M. Do for advice on physiological methods, T. Dunn for assistance with data analysis

software, and R. Helmiss for assistance with illustration. Funding was provided by NIH grants T32 EY007110 and F31 NS078893 (D.K.) and RO1 EY022073 (J.R.S.).

COMPETING INTERESTS

The authors declare no competing interests.

REFERENCES

Ackman, J.B., and Crair, M.C. (2014). Role of emergent neural activity in visual map development. Current opinion in neurobiology *24*, 166-175.

Bacci, A., Huguenard, J.R., and Prince, D.A. (2003). Functional autaptic neurotransmission in fast-spiking interneurons: a novel form of feedback inhibition in the neocortex. The Journal of neuroscience : the official journal of the Society for Neuroscience *23*, 859-866.

Baker, M.W., and Macagno, E.R. (2000). The role of a LAR-like receptor tyrosine phosphatase in growth cone collapse and mutual-avoidance by sibling processes. J Neurobio *44*, 194-203.

Barlow, H.B., and Hill, R.M. (1963). Selective sensitivity to direction of movement in ganglion cells of the rabbit retina. Science *139*, 412-414.

Bekkers, J.M., and Stevens, C.F. (1991). Excitatory and inhibitory autaptic currents in isolated hippocampal neurons maintained in cell culture. Proceedings of the National Academy of Sciences of the United States of America *88*, 7834-7838.

Briggman, K.L., Helmstaedter, M., and Denk, W. (2011). Wiring specificity in the direction-selectivity circuit of the retina. Nature *471*, 183-188.

Buffelli, M., Burgess, R.W., Feng, G., Lobe, C.G., Lichtman, J.W., and Sanes, J.R. (2003). Genetic evidence that relative synaptic efficacy biases the outcome of synaptic competition. Nature *424*, 430-434.

Burbridge, T.J., Xu, H.P., Ackman, J.B., Ge, X., Zhang, Y., Ye, M.J., Zhou, Z.J., Xu, J., Contractor, A., and Crair, M.C. (2014). Visual circuit development requires patterned activity mediated by retinal acetylcholine receptors. Neuron *84*, 1049-1064.

Chan, Y.C., and Chiao, C.C. (2013). The distribution of the preferred directions of the ON-OFF direction selective ganglion cells in the rabbit retina requires refinement after eye opening. Physiological reports *1*, e00013.

Chen, H., Liu, X., and Tian, N. (2014). Subtype-dependent postnatal development of direction- and orientation-selective retinal ganglion cells in mice. Journal of neurophysiology *112*, 2092-2101.

Crepel, F., Mariani, J., and Delhaye-Bouchard, N. (1976). Evidence for a multiple innervation of Purkinje cells by climbing fibers in the immature rat cerebellum. J Neurobio *7*, 567-578.

Duan, X., Krishnaswamy, A., De la Huerta, I., and Sanes, J.R. (2014). Type II cadherins guide assembly of a direction-selective retinal circuit. Cell *158*, 793-807.

Elstrott, J., Anishchenko, A., Greschner, M., Sher, A., Litke, A.M., Chichilnisky, E.J., and Feller, M.B. (2008). Direction selectivity in the retina is established independent of visual experience and cholinergic retinal waves. Neuron *58*, 499-506.

Enciso, G.A., Rempe, M., Dmitriev, A.V., Gavrikov, K.E., Terman, D., and Mangel, S.C. (2010). A model of direction selectivity in the starburst amacrine cell network. Journal of computational neuroscience *28*, 567-578.

663 Euler, T., Detwiler, P.B., and Denk, W. (2002). Directionally selective calcium signals in
664 dendrites of starburst amacrine cells. Nature *418*, 845-852.

665 Famiglietti, E.V. (1983). 'Starburst' amacrine cells and cholinergic neurons: mirror-symmetric
666 ON and OFF amacrine cells of rabbit retina. Brain Research *261*, 138-144.

667 Ford, K.J., Felix, A.L., and Feller, M.B. (2012). Cellular mechanisms underlying spatiotemporal
668 features of cholinergic retinal waves. The Journal of neuroscience : the official journal of the
669 Society for Neuroscience *32*, 850-863.

670 Fried, S.I., Munch, T.A., and Werblin, F.S. (2002). Mechanisms and circuitry underlying
671 directional selectivity in the retina. Nature *420*, 411-414.

672 Fuerst, P.G., Bruce, F., Tian, M., Wei, W., Elstrott, J., Feller, M.B., Erskine, L., Singer, J.H., and
673 Burgess, R.W. (2009). DSCAM and DSCAML1 function in self-avoidance in multiple cell types
674 in the developing mouse retina. Neuron *64*, 484-497.

675 Fuerst, P.G., Koizumi, A., Masland, R.H., and Burgess, R.W. (2008). Neurite arborization and
676 mosaic spacing in the mouse retina require DSCAM. Nature *451*, 470-474.

677 Gao, F.-B., Kohwi, M., Brenman, J.E., Jan, L.Y., and Jan, Y.N. (2000). Control of dendritic
678 formation in Drosophila: The roles of Flamingo and competition between homologous neurons.
679 Neuron *28*, 91-101.

680 Garrett, A.M., Schreiner, D., Lobas, M.A., and Weiner, J.A. (2012). gamma-protocadherins
681 control cortical dendrite arborization by regulating the activity of a FAK/PKC/MARCKS signaling
682 pathway. Neuron *74*, 269-276.

683 Gibson, D.A., Tymanskyj, S., Yuan, R.C., Leung, H.C., Lefebvre, J.L., Sanes, J.R., Chedotal, A.,
684 and Ma, L. (2014). Dendrite self-avoidance requires cell-autonomous slit/robo signaling in
685 cerebellar purkinje cells. Neuron *81*, 1040-1056.

686 Grueber, W.B., Graubard, K., and Truman, J.W. (2001). Tiling of the body wall by multidendritic
687 sensory neurons in Manduca sexta. 2001 *440*, 271-283.

688 Grueber, W.B., and Sagasti, A. (2010). Self-avoidance and tiling: Mechanisms of dendrite and
689 axon spacing. Cold Spring Harbor perspectives in biology *2*, a001750.

690 Grueber, W.B., Ye, B., Moore, A.W., Jan, L.Y., and Jan, Y.N. (2003). Dendrites of distinct
691 classes of Drosophila sensory neurons show different capacities of homotypic repulsion.
692 Current biology : CB *13*, 618-626.

693 Hattori, D., Chen, Y., Matthews, B.J., Salwinski, L., Sabatti, C., Grueber, W.B., and Zipursky,
694 S.L. (2009). Robust discrimination between self and non-self neurites requires thousands of
695 Dscam1 isoforms. Nature *461*, 644-648.

696 Hattori, D., Demir, E., Kim, H.W., Viragh, E., Zipursky, S.L., and Dickson, B.J. (2007). Dscam
697 diversity is essential for neuronal wiring and self-recognition. Nature *449*, 223-227.

698 Hayden, S.A., Mills, J.W., and Masland, R.H. (1980). Acetylcholine synthesis by displaced
699 amacrine cells. Science *210*, 435-437.

700 Helmstaedter, M., Briggman, K.L., Turaga, S.C., Jain, V., Seung, H.S., and Denk, W. (2013).
701 Connectomic reconstruction of the inner plexiform layer in the mouse retina. Nature *500*, 168-
702 174.

703 Hoggarth, A., McLaughlin, A.J., Ronellenfitch, K., Trenholm, S., Vasandani, R.,
704 Sethuramanujam, S., Schwab, D., Briggman, K.L., and Awatramani, G.B. (2015). Specific wiring
705 of distinct amacrine cells in the directionally selective retinal circuit permit independent encoding
706 of direction and size. Neuron *86*, 1-16.

707 Hughes, M.E., Bortnick, R., Tsubouchi, A., Baumer, P., Kondo, M., Uemura, T., and Schmucker,
708 D. (2007). Homophilic Dscam interactions control complex dendrite morphogenesis. Neuron *54*,
709 417-427.

710 Kaneko, R., Kato, H., Kawamura, Y., Esumi, S., Hirayama, T., Hirabayashi, T., and Yagi, T.
711 (2006). Allelic gene regulation of Pcdh-alpha and Pcdh-gamma clusters involving both
712 monoallelic and biallelic expression in single Purkinje cells. The Journal of biological chemistry
713 *281*, 30551-30560.

714 Kano, M., and Hashimoto, K. (2009). Synapse elimination in the central nervous system.
715 Current opinion in neurobiology *19*, 154-161.

716 Kay, J.N., De la Huerta, I., Kim, I.J., Zhang, Y., Yamagata, M., Chu, M.W., Meister, M., and
717 Sanes, J.R. (2011). Retinal ganglion cells with distinct directional preferences differ in molecular
718 identity, structure, and central projections. The Journal of neuroscience : the official journal of
719 the Society for Neuroscience *31*, 7753-7762.

720 Kim, I.J., Zhang, Y., Meister, M., and Sanes, J.R. (2010). Laminar restriction of retinal ganglion
721 cell dendrites and axons: subtype-specific developmental patterns revealed with transgenic
722 markers. The Journal of neuroscience : the official journal of the Society for Neuroscience *30*,
723 1452-1462.

724 Kim, I.J., Zhang, Y., Yamagata, M., Meister, M., and Sanes, J.R. (2008). Molecular identification
725 of a retinal cell type that responds to upward motion. Nature *452*, 478-482.

726 Kramer, A.P., and Kuwada, J.Y. (1983). Formation of receptive fields of leech mechanosensory
727 neurons during embryonic development. The Journal of neuroscience : the official journal of the
728 Society for Neuroscience *3*, 2474-2486.

729 Kramer, A.P., and Stent, G.S. (1985). Developmental arborization of sensory neurons in the
730 leech Haementeria ghilianii. II. Experimentally induced variations in the branching pattern. The
731 Journal of neuroscience : the official journal of the Society for Neuroscience *5*, 768-775.

732 Lee, S., and Zhou, Z.J. (2006). The synaptic mechanism of direction selectivity in distal
733 processes of starburst amacrine cells. Neuron *51*, 787-799.

734 Lefebvre, J.L., Kostadinov, D., Chen, W.V., Maniatis, T., and Sanes, J.R. (2012).
735 Protocadherins mediate dendritic self-avoidance in the mammalian nervous system. Nature
736 *488*, 517-521.

737 Lefebvre, J.L., Sanes, J.R., and Kay, J.N. (2015). Development of dendritic form and function.
738 Annu Rev Cell Dev Biol*, (in press)*.

739 Lefebvre, J.L., Zhang, Y., Meister, M., Wang, X., and Sanes, J.R. (2008). gamma-
740 Protocadherins regulate neuronal survival but are dispensable for circuit formation in retina.
741 Development *135*, 4141-4151.

742 Liu, Y., and Halloran, M.C. (2005). Central and peripheral axon branches from one neuron are
743 guided differentially by Semaphorin3D and transient axonal glycoprotein-1. The Journal of
744 neuroscience : the official journal of the Society for Neuroscience *25*, 10556-10563.

745 Long, H., Ou, Y., Rao, Y., and van Meyel, D.J. (2009). Dendrite branching and self-avoidance
746 are controlled by Turtle, a conserved IgSF protein in Drosophila. Development *136*, 3475-3484.

747 Madisen, L., Zwingman, T.A., Sunkin, S.M., Oh, S.W., Zariwala, H.A., Gu, H., Ng, L.L., Palmiter,
748 R.D., Hawrylycz, M.J., Jones, A.R.*, et al.* (2010). A robust and high-throughput Cre reporting
749 and characterization system for the whole mouse brain. Nature neuroscience *13*, 133-140.

750 Matsuoka, R.L., Jiang, Z., Samuels, I.S., Nguyen-Ba-Charvet, K.T., Sun, L.O., Peachey, N.S.,
751 Chedotal, A., Yau, K.W., and Kolodkin, A.L. (2012). Guidance-cue control of horizontal cell
752 morphology, lamination, and synapse formation in the mammalian outer retina. The Journal of
753 neuroscience : the official journal of the Society for Neuroscience *32*, 6859-6868.

754 Matthews, B.J., Kim, M.E., Flanagan, J.J., Hattori, D., Clemens, J.C., Zipursky, S.L., and
755 Grueber, W.B. (2007). Dendrite self-avoidance is controlled by Dscam. Cell *129*, 593-604.

756 Miura, S.K., Martins, A., Zhang, K.X., Graveley, B.R., and Zipursky, S.L. (2013). Probabilistic
757 splicing of Dscam1 establishes identity at the level of single neurons. Cell *155*, 1166-1177.

758 Montague, P.R., and Friedlander, M.J. (1991). Morphogenesis and territorial coverage by
759 isolated mammalian retinal ganglion cells. The Journal of neuroscience : the official journal of
760 the Society for Neuroscience *11*, 1440-1457.

761 Murata, Y., Hamada, S., Morishita, H., Mutoh, T., and Yagi, T. (2004). Interaction with
762 protocadherin-gamma regulates the cell surface expression of protocadherin-alpha. The Journal
763 of biological chemistry *279*, 49508-49516.

764 Murthy, V.N. (2011). Olfactory maps in the brain. Annual review of neuroscience *34*, 233-258.

765 Neves, G., Zucker, J., Daly, M., and Chess, A. (2004). Stochastic yet biased expression of
766 multiple Dscam splice variants by individual cells. Nature genetics *36*, 240-246.

767 Nicholls, J.G., and Baylor, D.A. (1968). Specific modalities and receptive fields of sensory
768 neurons in the CNS of the leech. Journal of neurophysiology *31*, 740-756.

769 Oyster, C.W., and Barlow, H.B. (1967). Direction-selective units in rabbit retina: distribution of
770 preferred directions. Science *155*, 841-842.

771 Park, S.J., Kim, I.J., Looger, L.L., Demb, J.B., and Borghuis, B.G. (2014). Excitatory synaptic
772 inputs to mouse on-off direction-selective retinal ganglion cells lack direction tuning. The Journal
773 of neuroscience : the official journal of the Society for Neuroscience *34*, 3976-3981.

774 Pfeffer, C.K., Xue, M., He, M., Huang, Z.J., and Scanziani, M. (2013). Inhibition of inhibition in
775 visual cortex: the logic of connections between molecularly distinct interneurons. Nature
776 neuroscience *16*, 1068-1076.

777 Prasad, T., Wang, X., Gray, P.A., and Weiner, J.A. (2008). A differential developmental pattern
778 of spinal interneuron apoptosis during synaptogenesis: insights from genetic analyses of the
779 protocadherin-gamma gene cluster. Development *135*, 4153-4164.

780 Purves, D., and Lichtman, J.W. (1980). Elimination of synapses in the developing nervous
781 system. Science *210*, 153-157.

782 Redfern, P.A. (1970). Neuromuscular transmission in new-born rats. J Physiol *209*, 701-709.

783 Rieubland, S., Roth, A., and Hausser, M. (2014). Structured connectivity in cerebellar inhibitory
784 networks. Neuron *81*, 913-929.

785 Rossi, J., Balthasar, N., Olson, D., Scott, M., Berglund, E., Lee, C.E., Choi, M.J., Lauzon, D.,
786 Lowell, B.B., and Elmquist, J.K. (2011). Melanocortin-4 receptors expressed by cholinergic
787 neurons regulate energy balance and glucose homeostasis. Cell metabolism *13*, 195-204.

788 Sagasti, A., Guido, M.R., Raible, D.W., and Schier, A.F. (2005). Repulsive interactions shape
789 the morphologies and functional arrangement of zebrafish peripheral sensory arbors. Current
790 biology : CB *15*, 804-814.

791 Schmucker, D., Clemens, J.E., Shu, H., Worby, C.A., Xiao, J., and Zipursky, S.L. (2000).
792 Drosophila Dscam is an axon guidance receptor exhibiting extraordinary molecular diversity.
793 Cell *101*, 671-684.

794 Schreiner, D., and Weiner, J.A. (2010). Combinatorial homophilic interaction between gamma-
795 protocadherin multimers greatly expands the molecular diversity of cell adhesion. Proceedings
796 of the National Academy of Sciences of the United States of America *107*, 14893-14898.

797 Smith, C.J., Watson, J.D., VanHoven, M.K., Colon-Ramos, D.A., and Miller, D.M., 3rd (2012).
798 Netrin (UNC-6) mediates dendritic self-avoidance. Nature neuroscience *15*, 731-737.

799 Soba, P., Zhu, S., Emoto, K., Younger, S., Yang, S.J., Yu, H.H., Lee, T., Jan, L.Y., and Jan,
800 Y.N. (2007). Drosophila sensory neurons require Dscam for dendritic self-avoidance and proper
801 dendritic field organization. Neuron *54*, 403-416.

802 Sun, L.O., Jiang, Z., Rivlin-Etzion, M., Hand, R., Brady, C.M., Matsuoka, R.L., Yau, K.W., Feller,
803 M.B., and Kolodkin, A.L. (2013). On and off retinal circuit assembly by divergent molecular
804 mechanisms. Science *342*, 1241974.

805 Tasic, B., Nabholz, C.E., Baldwin, K.K., Kim, Y., Rueckert, E.H., Ribich, S.A., Cramer, P., Wu,
806 Q., Axel, R., and Maniatis, T. (2002). Promoter choice determines splice site selection in
807 Protocadherin alpha and gamma pre-mRNA splicing. Molecular Cell *10*, 21-33.

808 Taylor, W.R., and Smith, R.G. (2012). The role of starburst amacrine cells in visual signal
809 processing. Visual neuroscience *29*, 73-81.

Taylor, W.R., and Vaney, D.I. (2002). Diverse synaptic mechanisms generate direction selectivity in the rabbit retina. The Journal of neuroscience : the official journal of the Society for Neuroscience *22*, 7712-7720.

Taylor, W.R., and Wassle, H. (1995). Receptive field properties of starburst cholinergic amacrine cells in the rabbit retina. European Journal of Neuroscience *7*, 2308-2321.

Thu, C.A., Chen, W.V., Rubinstein, R., Chevee, M., Wolcott, H.N., Felsovalyi, K.O., Tapia, J.C., Shapiro, L., Honig, B., and Maniatis, T. (2014). Single-cell identity generated by combinatorial homophilic interactions between alpha, beta, and gamma protocadherins. Cell *158*, 1045-1059.

Toyoda, S., Kawaguchi, M., Kobayashi, T., Tarusawa, E., Toyama, T., Okano, M., Oda, M., Nakauchi, H., Yoshimura, Y., Sanbo, M.*, et al.* (2014). Developmental epigenetic modification regulates stochastic expression of clustered protocadherin genes, generating single neuron diversity. Neuron *82*, 94-108.

Trenholm, S., Johnson, K., Li, X., Smith, R.G., and Awatramani, G.B. (2011). Parallel mechanisms encode direction in the retina. Neuron *71*, 683-694.

Vaney, D.I., Sivyer, B., and Taylor, W.R. (2012). Direction selectivity in the retina: symmetry and asymmetry in structure and function. Nature reviews Neuroscience *13*, 194-208.

Wang, J., Zugates, C.T., Liang, I.H., Lee, C.-H.J., and Lee, T. (2002a). Drosophila Dscam is required for divergent segregation of sister branches and suppresses ectopic bifurcation of axons. Neuron *33*, 559-571.

Wang, X., Weiner, J.A., Levi, S., Craig, A.M., Bradley, A., and Sanes, J.R. (2002b). Gamma Protocadherins are required for survival of spinal interneurons. Neuron *36*, 843-854.

Wassle, H., Puller, C., Muller, F., and Haverkamp, S. (2009). Cone contacts, mosaics, and territories of bipolar cells in the mouse retina. The Journal of neuroscience : the official journal of the Society for Neuroscience *29*, 106-117.

Weiner, J.A., Wang, X., Tapia, J.C., and Sanes, J.R. (2005). Gamma protocadherins are required for synaptic development in the spinal cord. Proceedings of the National Academy of Sciences of the United States of America *102*, 8-14.

Wichterle, H., Lieberam, I., Porter, J.A., and Jessell, T.M. (2002). Directed differentiation of embryonic stem cells into motor neurons. Cell *110*, 385-397.

Wojtowicz, W.M., Flanagan, J.J., Millard, S.S., Zipursky, S.L., and Clemens, J.C. (2004). Alternative splicing of Drosophila Dscam generates axon guidance receptors that exhibit isoform-specific homophilic binding. Cell *118*, 619-633.

Wojtowicz, W.M., Wu, W., Andre, I., Qian, B., Baker, D., and Zipursky, S.L. (2007). A vast repertoire of Dscam binding specificities arises from modular interactions of variable Ig domains. Cell *130*, 1134-1145.

Yau, K.-W. (1976). Receptive fields, geometry and conduction block of sensory neurones in the central nervous system of the leech. Journal of physiology *263*, 513-538.

847 Yonehara, K., Balint, K., Noda, M., Nagel, G., Bamberg, E., and Roska, B. (2011). Spatially
848 asymmetric reorganization of inhibition establishes a motion-sensitive circuit. Nature *469*, 407-
849 410.

850 Yonehara, K., Farrow, K., Ghanem, A., Hillier, D., Balint, K., Teixeira, M., Juttner, J., Noda, M.,
851 Neve, R.L., Conzelmann, K.K.*, et al.* (2013). The first stage of cardinal direction selectivity is
852 localized to the dendrites of retinal ganglion cells. Neuron *79*, 1078-1085.

853 Yoshida, K., Watanabe, D., Ishikane, K., Tachibana, M., Pastan, I., and Nakanishi, S. (2001). A
854 key role of starburst amacrine cells in originating retina directional selectivity and optokinetic eye
855 movement. Neuron *30*, 771-780.

856 Zhan, X.L., Clemens, J.C., Neves, G., Hattori, D., Flanagan, J.J., Hummel, T., Vasconcelos,
857 M.L., Chess, A., and Zipursky, S.L. (2004). Analysis of Dscam diversity in regulating axon
858 guidance in Drosophila mushroom bodies. Neuron *43*, 673-686.

859 Zheng, J.J., Lee, S., and Zhou, Z.J. (2004). A developmental switch in the excitability and
860 function of the starburst network in the mammalian retina. Neuron *44*, 851-864.

861 Zipursky, S.L., and Grueber, W.B. (2013). The molecular basis of self-avoidance. Annual review
862 of neuroscience *36*, 547-568.

863

FIGURE LEGENDS

Figure 1: Pcdhg-dependent self-avoidance and self/non-self discrimination in SACs

A. Self-avoiding neurites lack isoneuronal contacts (repulsion) but adhere to and can form synapses with neurites of other cells of the same type, displaying self/non-self discrimination (adhesion).

B. Schematic of *Pcdhg* genomic locus and protein product. Distinct Pcdhg isoforms are assembled by splicing one of 22 variable exons, encoding the extracellular and transmembrane portions of the protein, to three constant exons, encoding the intracellular portion of the protein.

C. Vertical section of retina stained against ChAT to label all SACs (gray) overlaid with cartooned individual OFF and ON SACs (red). OFF SAC cell bodies reside in the inner nuclear layer (INL) and ON SAC cell bodies reside in the ganglion cell layer (GCL). SAC neurites reside in the inner plexiform layer (IPL).

D. *En face* view of individual dye-filled ON SAC in $Pcdhg^{22}$ retina.

E. Schematic of the retinal direction-selective circuit components and connections. PRs, photoreceptors; BCs, bipolar cells; SACs, starburst amacrine cells; DSGC, direction-selective ganglion cell. Gray stripes indicate OFF and ON direction-selective sublaminae (S2 and S4, respectively). Green and red arrows indicate directional preferences of DSGCs and SAC dendrites, respectively.

F. – H. Schematic representation of the effects of changing Pcdhg expression in SACs (summary from Lefebvre et al., 2012). SACs from $Pcdhg^{22}$ retinas (**F**) are posited to express unique subsets of Pcdhgs and thus exhibit both self-avoidance and non-self adhesion. SACs from $Pcdhg^{0}$ retinas (**G**) express no Pcdhgs and thus do not exhibit self-avoidance. SACs from $Pcdhg^{1}$ retinas (**H**) all express the same Pcdhg and thus exhibit self-avoidance but not non-self adhesion.

Scale bar = 50 μm in **C** and **D**.

Figure 2: SAC-SAC connections in Pcdhg^{22} and Pcdhg^{0} retinas

A. Paired recording configuration: SACs at various intercellular distances were targeted for recording in Pcdhg^{22} (left) and Pcdhg^{0} (right) retinas. Imaged are tracings of real SACs.

B. – E. Presynaptic voltage steps from V_h = -70 to +20 mV (top) and examples of currents recorded from both pre- and postsynaptic pairs of SACs that were connected (middle) and not connected (bottom) in juvenile Pcdhg^{22} retinas (**B**), adult Pcdhg^{22} retinas (**C**), juvenile Pcdhg^{0} retinas (**D**), and adult Pcdhg^{0} retinas (**E**).

F. – I. Scatter plots of intercellular distance versus peak current size in juvenile Pcdhg^{22} retinas (**F**), adult Pcdhg^{22} retinas (**G**), juvenile Pcdhg^{0} retinas (**H**), and adult Pcdhg^{0} retinas (**I**). Number of connections tested = 34, 35, 37, and 39 in **F-I**, respectively.

J. Average peak current in connected SAC pairs at P15-24 (left) and P40-100 (right). Number of connections recorded = 21, 9, 23, and 20 in juvenile Pcdhg^{22} retinas, adult Pcdhg^{22} retinas, juvenile Pcdhg^{0} retinas, and adult Pcdhg^{0} retinas, respectively.

K. Distance dependence of SAC-SAC connectivity at in P15-24 animals (left) and P40-100 animals (right).

Data are shown as mean ± S.E.M. Statistics: n.s. = not significant, *P < .05, ** P < .01. See also Figure 2 – figure supplements 1-4.

Figure 3: Pcdhg^{0} SACs form autapses

A. SAC autaptic voltage stimulus (left). Single SAC recording configuration in Pcdhg^{22} (middle) and Pcdhg^{0} (right) retinas.

B. – E. Example currents recorded from SACs in juvenile Pcdhg^{22} retinas (**B**), juvenile Pcdhg^{0} retinas (**C**), adult Pcdhg^{22} retinas (**D**) and adult Pcdhg^{0} retinas (**E**) in response to voltage stimulus shown in **A**. Arrowheads in **C** and **E** points to autaptic currents in SAC from Pcdhg^{0} retinas that were blocked by 50 µM picrotoxin (blue trace in **C**). Gray bars indicate

depolarization steps to +60 mV (stimulus artifacts) that were 2 ms long in both **B**, **C**, and **D**, and 4 ms long in **E**. The shorter latency in **E** likely reflects the longer depolarization step. Full traces are shown as insets with enlarged regions outlined in magenta.

F. Peak outward currents measured during falling phase recorded current after initial voltage-step to +60 mV. Data points are staggered slightly for visual clarity. Number of SACs recorded = 8, 8, 7, and 6 in juvenile $Pcdhg^{22}$ retinas, juvenile $Pcdhg^{0}$ retinas, adult $Pcdhg^{22}$ retinas, and adult $Pcdhg^{0}$ retinas, respectively.

G. Average peak autaptic currents evoked in SACs from $Pcdhg^{0}$ retinas at P21-24 (left) and P40-100 (right) at V_h = -20 mV.

Data are shown as mean ± S.E.M. See also Figure 3 – figure supplement 1.

Figure 4: Decreased SAC-SAC connections in $Pcdhg^{1}$ retina

A. Replacement of all 22 Pcdhgs in SACs with a single Pcdhg isoform (top) rescues self-avoidance in individual SACs (bottom).

B. Plexus of all SAC dendrites (stained with anti-ChAT) in $Pcdhg^{22}$ (left), $Pcdhg^{0}$ (middle), and $Pcdhg^{1}$ (right) retinas.

C. Presynaptic voltage steps from V_h = -70 to +20 mV (top) and examples of currents recorded from both pre- and postsynaptic pairs of SACs that were connected (middle) and not connected (bottom) in juvenile $Pcdhg^{1}$ retinas.

D. – E. Scatter plots of intercellular distance versus peak current size in juvenile (**D**) and adult (**E**) $Pcdhg^{1}$ retinas.

F. Percent of P15-24 recorded SAC pairs that were connected, irrespective of intercellular distance. Number of connections tested = 34, 37, and 19 in $Pcdhg^{22}$, $Pcdhg^{0}$, and $Pcdhg^{1}$ retinas, respectively.

G. Same as **F** for adult retinas. Number of connections tested = 35, 39, and 13 in $Pcdhg^{22}$, $Pcdhg^{0}$, and $Pcdhg^{1}$ retinas, respectively.

H. Average peak current in connected SAC pairs at all ages. Number of recorded connections = 30, 43, and 3 in $Pcdhg^{22}$, $Pcdhg^{0}$, and $Pcdhg^{1}$ retinas, respectively.

Scale bar = 50 μm in **A** and 25 μm in **B**. Data are shown as mean ± S.E.M. Statistics: ** P < .01.

Figure 5: Integration of SACs into a direction-selective circuit is Pcdhg-independent.

A. Schematic of excitatory and inhibitory synaptic inputs of retinal direction-selective circuit, showing bipolar inputs to SACs (measured in **B** and **C**), SAC inputs to DSGCs (measured in **D** and **E**), and bipolar inputs to DSGCs (measured in **F** and **G**).

B. Example excitatory currents (V_h = -70 mV) of ON SACs from $Pcdhg^{22}$ (black), $Pcdhg^{0}$ (gray), and $Pcdhg^{1}$ (red) retinas evoked by a bright spot flash.

C. Average peak current responses to the onset of flash stimulus. Number of SACs recorded is 8, 9, and 7 in $Pcdhg^{22}$, $Pcdhg^{0}$, and $Pcdhg^{1}$ retinas, respectively.

D. Example inhibitory currents (V_h = 0 mV) of vDSGCs from $Pcdhg^{22}$, $Pcdhg^{0}$, and $Pcdhg^{1}$ retinas evoked by the onset (left) and offset (right) of a bright spot flash.

E. Average peak current responses to the onset (left) and offset (right) of flash stimulus. Number of vDSGCs recorded is 12, 13, and 10 in $Pcdhg^{22}$, $Pcdhg^{0}$, and $Pcdhg^{1}$ retinas, respectively.

F. Example excitatory currents (V_h = -70 mV) of vDSGCs from $Pcdhg^{22}$, $Pcdhg^{0}$, and $Pcdhg^{1}$ retinas evoked by the onset (left) and offset (right) of a 2 second bright spot flash.

G. Average peak current responses to the onset (left) and offset (right) of flash stimulus. Number of vDSGCs recorded is 14, 11, and 13 in $Pcdhg^{22}$, $Pcdhg^{0}$, and $Pcdhg^{1}$ retinas, respectively.

H. – J. Dye-filled vDSGCs with OFF and ON arborizations separated (top and middle, respectively) in $Pcdhg^{22}$ (**H**), $Pcdhg^{0}$ (**I**), and $Pcdhg^{1}$ (**J**) retinas. Bottom panels: Overlay of ON vDSGC dendrites (green) with ON SAC dendrites labeled with anti-ChAT antibody (red). Similar co-fasciculation was seen for OFF dendrites. Scale bar = 50 μm.

968 Data are shown as mean ± S.E.M. Spot flashes were displayed for 2 seconds in each case. See
969 also Figure 5 – figure supplement 1.
970
971 **Figure 6: Alteration of Pcdhg expression degrades direction selectivity**
972 **A.** Spiking responses of vDSGC from adult $Pcdhg^{22}$ retina to a bright moving bar moving in 8
973 directions. Polar plot is of peak firing rates in response to bar entering (ON, green) and
974 exiting (OFF, blue) the receptive field center. Vectors represent vector sum direction-
975 selective indices (DSIs) of ON and OFF responses. Surrounding central plot are spike
976 histograms used to make polar plot and calculate DSIs and preferred directions.
977 **B.** ON (left, green) and OFF (right, blue) DSI vectors for all recorded DSGCs in $Pcdhg^{22}$ retina
978 (n = 28 cells). Axes of retina are indicated with compass arrows: D, V, N, and T represent
979 dorsal, ventral, nasal, and temporal.
980 **C. - D.** Same as A and B but from adult $Pcdhg^{0}$ retinas (n = 28 cells).
981 **E. - F.** Same as A and B but from adult $Pcdhg^{1}$ retinas (n = 19 cells).
982 **G.** Mean absolute DSI for all cells recorded, irrespective of which direction they preferred.
983 **H.** Mean angle deviated from ventral direction for all cells recorded.
984 **I.** Mean absolute difference between DSI (left) and angle of preference (right) for all recorded
985 cells.
986 **J.** Plot of mean ventral projections of DSI vectors. For each recorded vDSGC, maximal ON
987 and OFF firing rates in each direction were summed and used to generate a single DSI
988 vector for each cell.
989 Data are shown as mean ± S.E.M. Statistics: n.s. = not significant, *P < .05, ** P < .01, *** P <
990 .001. See also Figure 6 – figure supplements 1-2.
991
992 **Figure 7: Synaptic basis of degraded direction selectivity in $Pcdhg^{0}$, and $Pcdhg^{1}$ retinas**

A. Example excitatory (black, V_h = -70 mV) and inhibitory (gray, V_h = 0 mV) currents evoked by leading edge (ON response) of bar moving in ventral (left) and dorsal (right) directions in vDSGC from $Pcdhg^{22}$ retina.

B. Examples of relative timing of excitation and inhibition in same cell from panel **A**.

C. Schematic of inhibitory input to vDSGCs in $Pcdhg^{22}$ retinas. vDSGCs receive inhibitory input from SAC dendrites with predominately dorsal orientations and directional preferences, setting the null direction of vDSGCs. These SAC dendrites, in turn, receive inhibitory input from SAC dendrites with predominately ventral orientation and preference, suppressing inhibition to vDSGCs during ventral motion through inhibition of inhibition.

D. – E. Same as **A-B** but in $Pcdhg^{0}$ retina.

F. Schematic of inhibitory input to vDSGCs in $Pcdhg^{0}$ retinas. vDSGCs receive inhibitory input from curvilinear SAC dendrites with disrupted orientations and directional preferences, diminishing their ability to set the null direction of vDSGCs. These SAC dendrites, in turn, receive inhibitory input from both parallel and antiparallel SAC dendrites.

G. – H. Same as **A-B** but for trailing edge (OFF response) in $Pcdhg^{1}$ retina.

I. Schematic of inhibitory input to vDSGCs in $Pcdhg^{1}$ retinas. vDSGCs receive inhibitory input from SAC dendrites with predominately dorsal orientations and directional preferences, setting the null direction of vDSGCs. These SAC dendrites, however, are no longer inhibited by SAC dendrites with predominately ventral orientation and preference, so their input to vDSGCs during ventral motion is not suppressed.

J. Ratio of peak excitatory current sizes evoked in vDSGCs by ventral versus dorsal motion in $Pcdhg^{22}$ (black), $Pcdhg^{0}$ (gray), and $Pcdhg^{1}$ (red) retinas.

K. Same as **J** but for inhibitory currents.

L. Relative timing of onset of excitation compared to inhibition during ventral motion in $Pcdhg^{22}$ (black), $Pcdhg^{0}$ (gray), and $Pcdhg^{1}$ (red) retinas.

M. Same as **L** but during dorsal motion.

1019 Data are shown as mean ± S.E.M. Number of recorded vDSGCs = 14, 10, and 13 in $Pcdhg^{22}$,
1020 $Pcdhg^{0}$, and $Pcdhg^{1}$ retinas. Leading edge (ON) and trailing edge (OFF) responses were
1021 measured for all cells and used as independent data points for quantification. Statistics: n.s. =
1022 not significant, *P < .05, ** P < .001.

FIGURE SUPPLEMENT LEGENDS

Figure 2 – figure supplement 1: Recording distances and SAC dendritic radii

A. Cumulative histogram of intercellular distances of SAC connections that were tested in juvenile animals (left) and adult animals (right). Histogram range is 25-175 μm with bins of 10 μm. Number of connections tested = 34, 37, 19, 35, 39, and 13 for P15-24 $Pcdhg^{22}$, P15-24 $Pcdhg^{0}$, P15-24 $Pcdhg^{1}$, P40-100 $Pcdhg^{22}$, P40-100 $Pcdhg^{0}$ SACs, and P40-100 $Pcdhg^{1}$ SACs, respectively.

B. Top: Histograms of dendritic radii of $Pcdhg^{22}$, $Pcdhg^{0}$, and $Pcdhg^{1}$ SACs. Bottom: Average dendritic radii across conditions. These measurements are from living retinas; following fixation, staining, and mounting, the dendritic radius of SACs is ~25% larger, as reported in many anatomical studies.

C. Relationship between intercellular distance and amount of dendritic overlap (SAC modeled as 100 μm radius circles).

Figure 2 – figure supplement 2: Characterization of SAC-SAC synaptic connections

A. Left: Histogram of synaptic latencies in all connected cells. Histogram range is 0-20 ms after presynaptic depolarization, and bin size is 2 ms. Right: Same analysis performed on non-connected pairs with histogram range of 0-50 ms and bin size 2 ms.

B. Two examples of SAC paired recording showing that application of 50 μM Picrotoxin eliminates transmission in these pairs, and thus currents GABAergic. Presynaptic cells were stepped from Vh = -70 to +20 mV. Postsynaptic cells were held at Vh = +30 mV.

C. Average current-voltage relationship of SAC-SAC connections, showing reversal at E_{Cl} (n = 3 pairs).

D. Monte Carlo simulations of paired SAC recordings to assess the specificity of reciprocal connections. Each gray histogram was generated from 10^5 simulations using experimentally determined connection probabilities. Experimentally observed values are indicated by cyan

arrows. Top: Comparison of observed values with simulations for all reciprocal connections recorded in Pcdhg^{22} retinas. Unidirectional connections are significantly underrepresented in our data set. Bottom: Comparison of observed values with simulations for all reciprocal connections recorded across all conditions. Unidirectional connections are significantly underrepresented in our data set, and non-connected pairs are significantly overrepresented in our data set.

Statistics: n.s. = not significant, *P < .05, ** P < .01.

Figure 2 – figure supplement 3: Lamination and spacing of SACs are normal in Pcdhg^{0}, and Pcdhg^{1} retinas

A. Vertical section of retina stained against ChAT to label all SACs in Pcdhg^{22}, Pcdhg^{0}, and Pcdhg^{1} retinas (left to right). Scale bar = 50 μm.

B. Top: *En face* view of OFF SACs in Pcdhg^{22}, Pcdhg^{0}, and Pcdhg^{1} retinas (left to right, respectively). Scale bar = 100 μm. Bottom: Density recovery profile of OFF SACs in Pcdhg^{22}, Pcdhg^{0}, and Pcdhg^{1} retinas (left) and total OFF SAC density.

C. Same as B but for ON SACs.

Figure 2 – figure supplement 4: Normal retinal morphology in Pcdhg^{0}, and Pcdhg^{1} retinas

A. Nuclear label of all retinal neurons (TO-PRO3) showing retinal thickness is similar across conditions. Whole retinal thickness is shown.

B. Anti-Chx10 immunostaining to label bipolar cells. Image is cropped to just show inner nuclear layer.

C. Anti-AP2 immunostaining to label amacrine cells. Image is cropped to just show inner nuclear layer through ganglion cell layer. Some retinal blood vessels were also labeled because primary antibody is mouse monoclonal.

D. Anti-Brn3a immunostaining to label many retinal ganglion cells. Image is cropped to just show ganglion cell layer.

E. Anti-Calbindin immunostaining to label horizontal cells, some amacrine cells, and some retinal ganglion cells. Image is cropped to just show outer plexiform layer through ganglion cell layer.

All images show examples from P21 $Pcdhg^{22}$, $Pcdhg^{0}$, and $Pcdhg^{1}$ vertical retinal sections in parallel (left to right, respectively). Scale bar = 50 μm in all panels. Images are oriented with photoreceptors towards the top and retinal ganglion cells toward the bottom of the page.

Figure 3 – figure supplement 1: Quantification of autaptic currents

A. Example of paired recording using 'autaptic' voltage stimulus, showing that brief depolarization can evoke transmission in pairs of neurons.

B. Top: Example current recordings of $Pcdhg^{22}$ (left) and $Pcdhg^{0}$ SACs in response to autaptic voltage stimulus. Bottom: insets from top panel showing averaged responses (black) and 4 raw traces in each condition (gray).

C. Comparison of synaptic and autaptic properties in SACs showing similarity in latency, rise time, and Picrotoxin sensitivity. Data are shown as mean ± S.D.

Figure 5 – figure supplement 1: Normal expression, spacing, and number of vDSGCs in $Pcdhg^{0}$, and $Pcdhg^{1}$ retinas

A. Anti-GFP immunostaining in HB9-GFP positive retinas. Note that GFP signal is faint in dendrites by P21 but retained in cell body. Image is cropped to show inner nuclear layer through ganglion cell layer.

B. Anti-CART immunostaining in same sections from A to label all populations of DSGCs.

C. Merge of panels **A** and **B** showing that HB9-GFP positive vDSGCs are positive for CART, but not the only CART positive cells in the ganglion cell layer. Note that CART antibody also labels Tyrosine hydroxylase-positive amacrine cells strongly in retinal sublamina 1.

D. Top: En face view of field of HB9-positive vDSGCs (inverted contrast). Bottom: Density recovery profile of HB9-GFP positive vDSGCs in $Pcdhg^{22}$, $Pcdhg^{0}$, and $Pcdhg^{1}$ retinas (left) and total HB9-GFP positive vDSGC density.

All images show examples from P21 $Pcdhg^{22}$, $Pcdhg^{0}$, and $Pcdhg^{1}$ retinas in parallel (left to right, respectively). Scale bar = 50 μm in panels **A-C** and 100 μm in panel **D**. Images in panels **A-C** are vertical retinal sections oriented such that photoreceptors are towards the top of the page.

Figure 6 – figure supplement 1: ON and OFF direction responses of vDSGCs are similarly blunted when Pcdhg expression in SACs is altered

A. Cumulative histogram of ON and OFF direction-selective indices (top) and angle away from ventral (bottom) for all recorded vDSGCs in $Pcdhg^{22}$, $Pcdhg^{0}$, and $Pcdhg^{1}$ retinas (n = 28, 28, and 19, respectively). Histogram bins are .05 DSI units and 10 degrees for top and bottom panels, respectively.

B. Ratios of excitatory (left) and inhibitory (right) ON and OFF current sizes (ventral over dorsal motion) for all recorded cells in $Pcdhg^{22}$, $Pcdhg^{0}$, and $Pcdhg^{1}$ retinas (Excitatory n = 14, 10, and 10 ON and OFF each, respectively; Inhibitory n = 14, 10, and 13 ON and OFF each, respectively).

C. Relative timing of ON and OFF excitation compared to inhibition during ventral motion (left) and dorsal motion (right) for all recorded cells in $Pcdhg^{22}$, $Pcdhg^{0}$, and $Pcdhg^{1}$ retinas (n = 12, 8, and 8 ON and OFF each, respectively).

ON and OFF responses are shown in green and blue, respectively. Statistics: n.s. = not significant.

Figure 6 – figure supplement 2: Age-dependent improvement in direction selectivity of vDSGCs requires Pcdhgs

A. Comparison of DSI of juvenile and adult vDSGCs in $Pcdhg^{22}$ and $Pcdhg^{0}$ retinas.

B. Comparison of deviations from ventral of juvenile and adult vDSGCs $Pcdhg^{22}$ and $Pcdhg^{0}$ retinas.

Statistics: n.s. = not significant, *P < .05, ** P < .0005. n = 10 and 6 for P15-24 $Pcdhg^{22}$ and $Pcdhg^{0}$ vDSGCs, respectively, and n = 28 and 28 for adult $Pcdhg^{22}$ and $Pcdhg^{0}$ vDSGCs, respectively. Leading edge (ON) and trailing edge (OFF) responses were measured for all cells and used as independent data points.

SOURCE CODE

Source code 1 – Visual stimuli

Source code 2 – Microscope acquisition

Source code 3 – Electrophysiology analysis

Figure 1

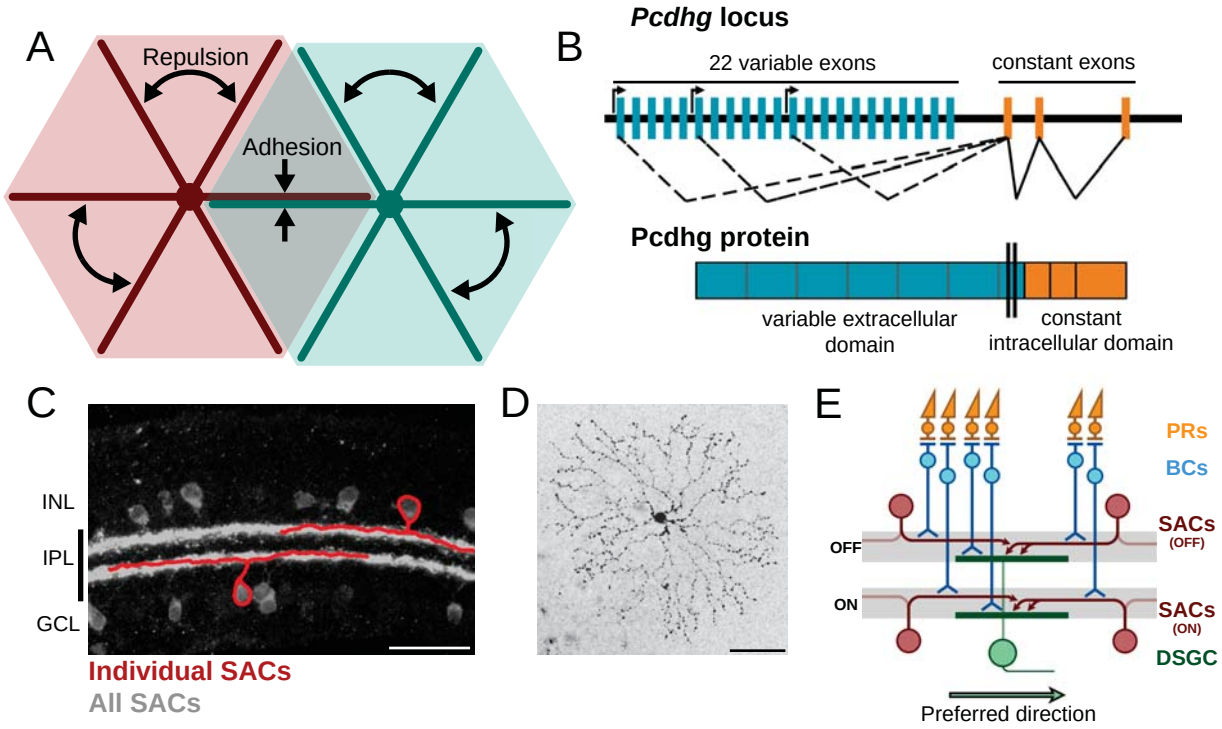
A
Repulsion
Adhesion
B
Pcdhg locus
22 variable exons
constant exons
Pcdhg protein
variable extracellular domain
constant intracellular domain
C
INL
IPL
GCL
Individual SACs
All SACs
D
E
PRs
BCs
SACs (OFF)
OFF
ON
SACs (ON)
DSGC
Preferred direction
F
Pcdhg22 SACs
Self-avoidance
Non-self adhesion
G
Pcdhg0 SACs
~~Self-avoidance~~
Non-self adhesion
H
Pcdhg1 SACs
Self-avoidance
~~Non-self adhesion~~

Figure 2

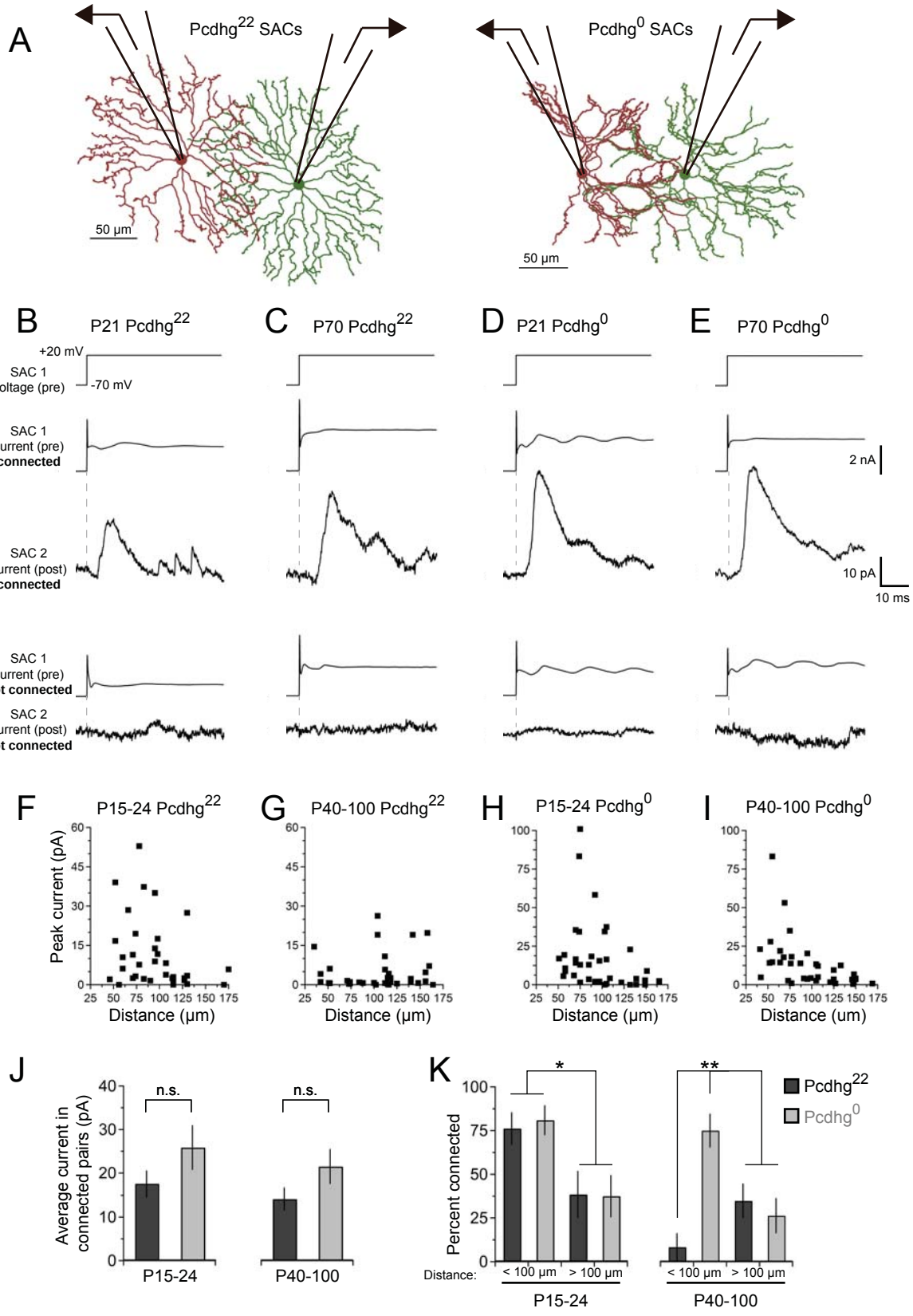
A
Pcdhg22 SACs
Pcdhg0 SACs
50 µm
50 µm
B
P21 Pcdhg22
C
P70 Pcdhg22
D
P21 Pcdhg0
E
P70 Pcdhg0
+20 mV
SAC 1 voltage (pre)
-70 mV
SAC 1 current (pre) connected
SAC 2 current (post) connected
2 nA
10 pA
10 ms
SAC 1 current (pre) not connected
SAC 2 current (post) not connected
F
P15-24 Pcdhg22
G
P40-100 Pcdhg22
H
P15-24 Pcdhg0
I
P40-100 Pcdhg0
Peak current (pA)
Distance (µm)
Distance (um)
J
Average current in connected pairs (pA)
n.s.
n.s.
P15-24
P40-100
K
Percent connected
*
**
Pcdhg22
Pcdhg0
Distance:
< 100 µm
> 100 µm
P15-24
P40-100

Figure 3

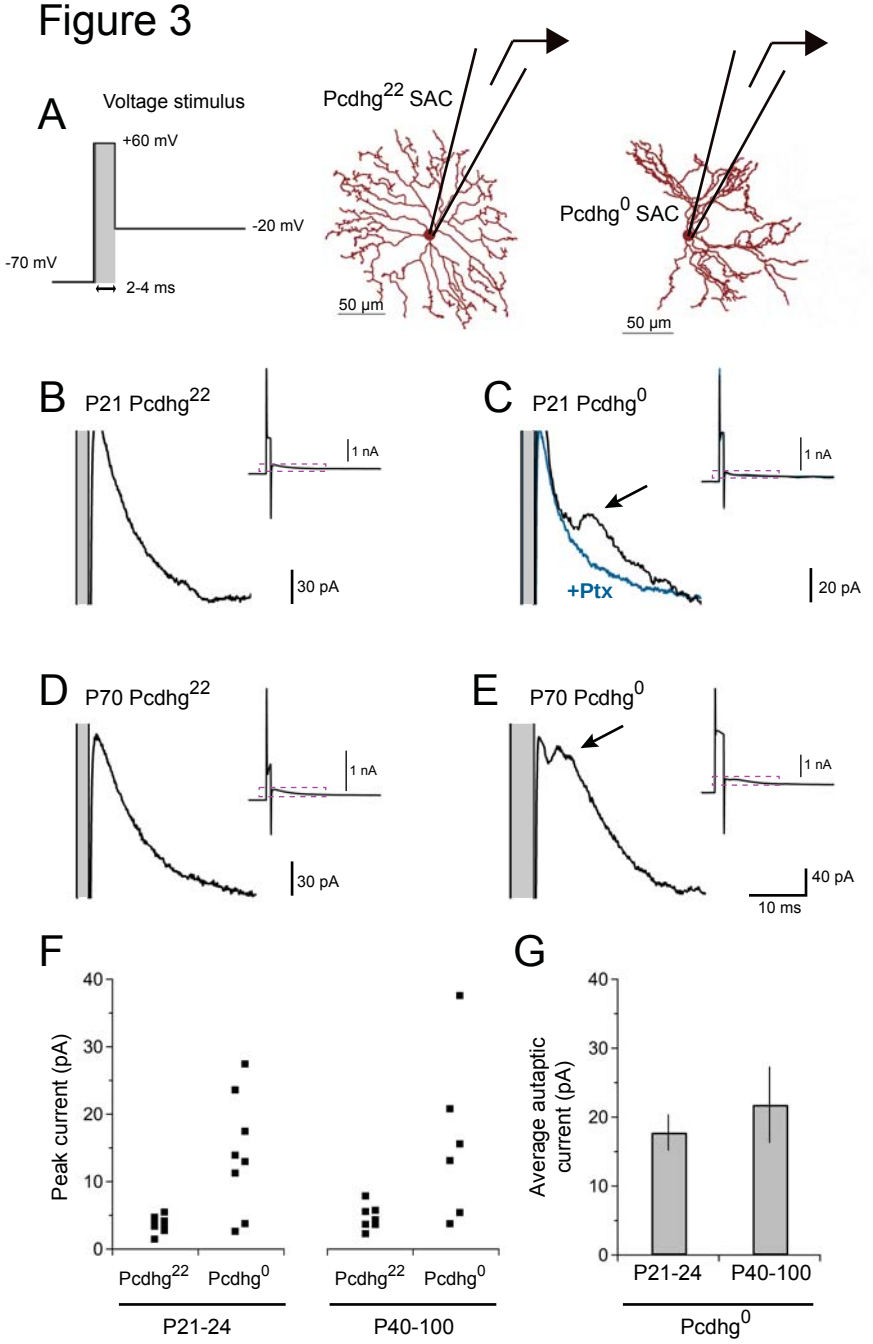
A
Voltage stimulus
+60 mV
-20 mV
-70 mV
2-4 ms
Pcdhg22 SAC
50 µm
Pcdhg0 SAC
50 µm
B
P21 Pcdhg22
1 nA
30 pA
C
P21 Pcdhg0
1 nA
+Ptx
20 pA
D
P70 Pcdhg22
1 nA
30 pA
E
P70 Pcdhg0
1 nA
40 pA
10 ms
F
Peak current (pA)
40
30
20
10
0
Pcdhg22
Pcdhg0
Pcdhg22
Pcdhg0
P21-24
P40-100
G
Average autaptic current (pA)
40
30
20
10
0
P21-24
P40-100
Pcdhg0

Figure 4

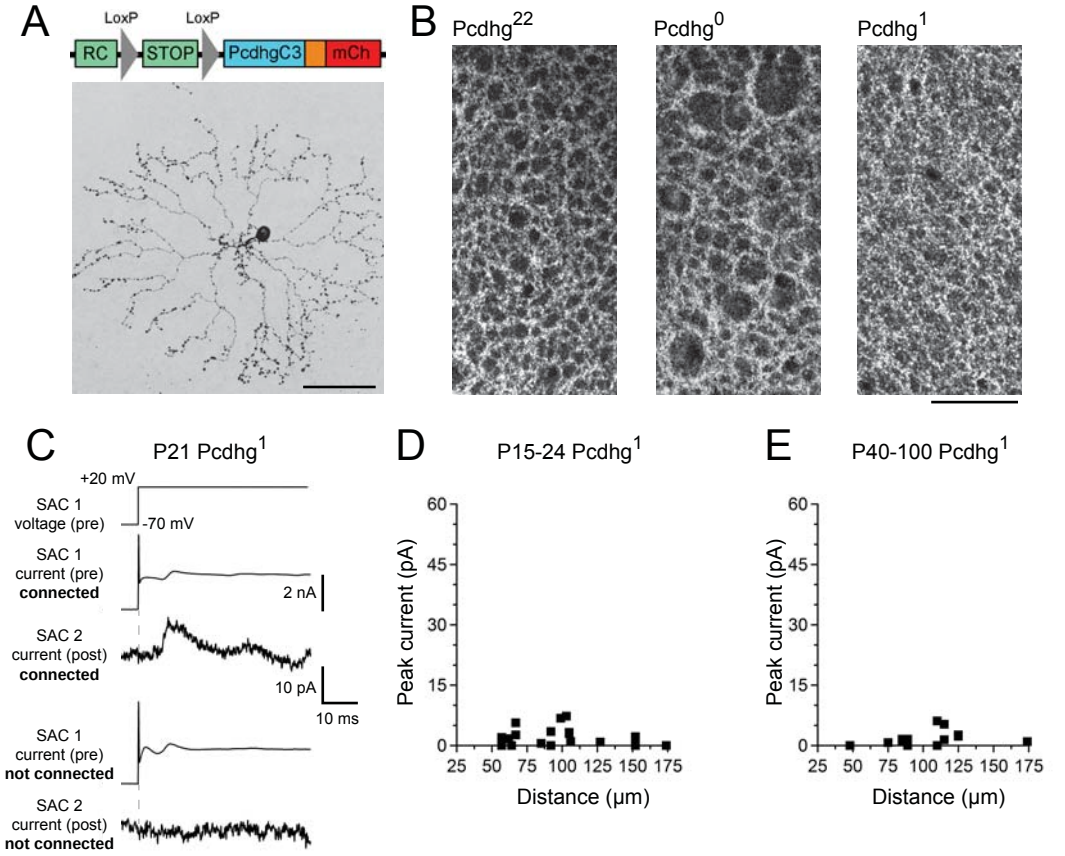
A
LoxP
LoxP
RC
STOP
PcdhgC3
mCh
B
Pcdhg22
Pcdhg0
Pcdhg1
C
P21 Pcdhg1
+20 mV
SAC 1
voltage (pre)
-70 mV
SAC 1
current (pre)
connected
2 nA
SAC 2
current (post)
connected
10 pA
10 ms
SAC 1
current (pre)
not connected
SAC 2
current (post)
not connected
D
P15-24 Pcdhg1
Peak current (pA)
Distance (μm)
E
P40-100 Pcdhg1
Peak current (pA)
Distance (μm)
F
Percent connected
Pcdhg22 Pcdhg0 Pcdhg1
P21-24
G
Percent connected
Pcdhg22 Pcdhg0 Pcdhg1
P40-100
H
Average current in connected pairs (pA)
Pcdhg22 Pcdhg0 Pcdhg1

Figure 5

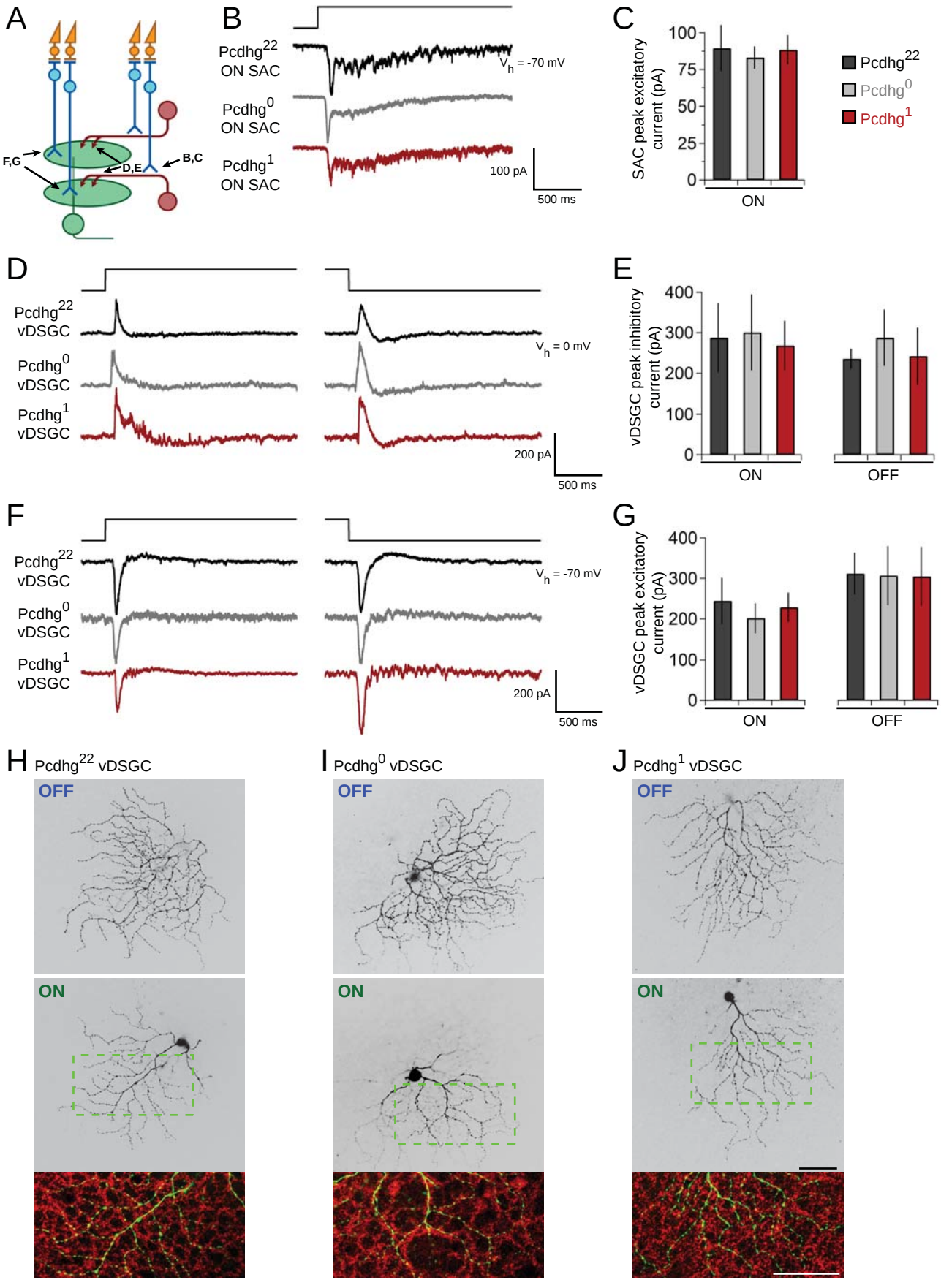
A
F,G
D,E
B,C
B
Pcdhg22 ON SAC
Pcdhg0 ON SAC
Pcdhg1 ON SAC
Vh = -70 mV
100 pA
500 ms
C
SAC peak excitatory current (pA)
100
75
50
25
0
ON
Pcdhg22
Pcdhg0
Pcdhg1
D
Pcdhg22 vDSGC
Pcdhg0 vDSGC
Pcdhg1 vDSGC
Vh = 0 mV
200 pA
500 ms
E
vDSGC peak inhibitory current (pA)
400
300
200
100
0
ON
OFF
F
Pcdhg22 vDSGC
Pcdhg0 vDSGC
Pcdhg1 vDSGC
Vh = -70 mV
200 pA
500 ms
G
vDSGC peak excitatory current (pA)
400
300
200
100
0
ON
OFF
H Pcdhg22 vDSGC
I Pcdhg0 vDSGC
J Pcdhg1 vDSGC
OFF
ON

Figure 6

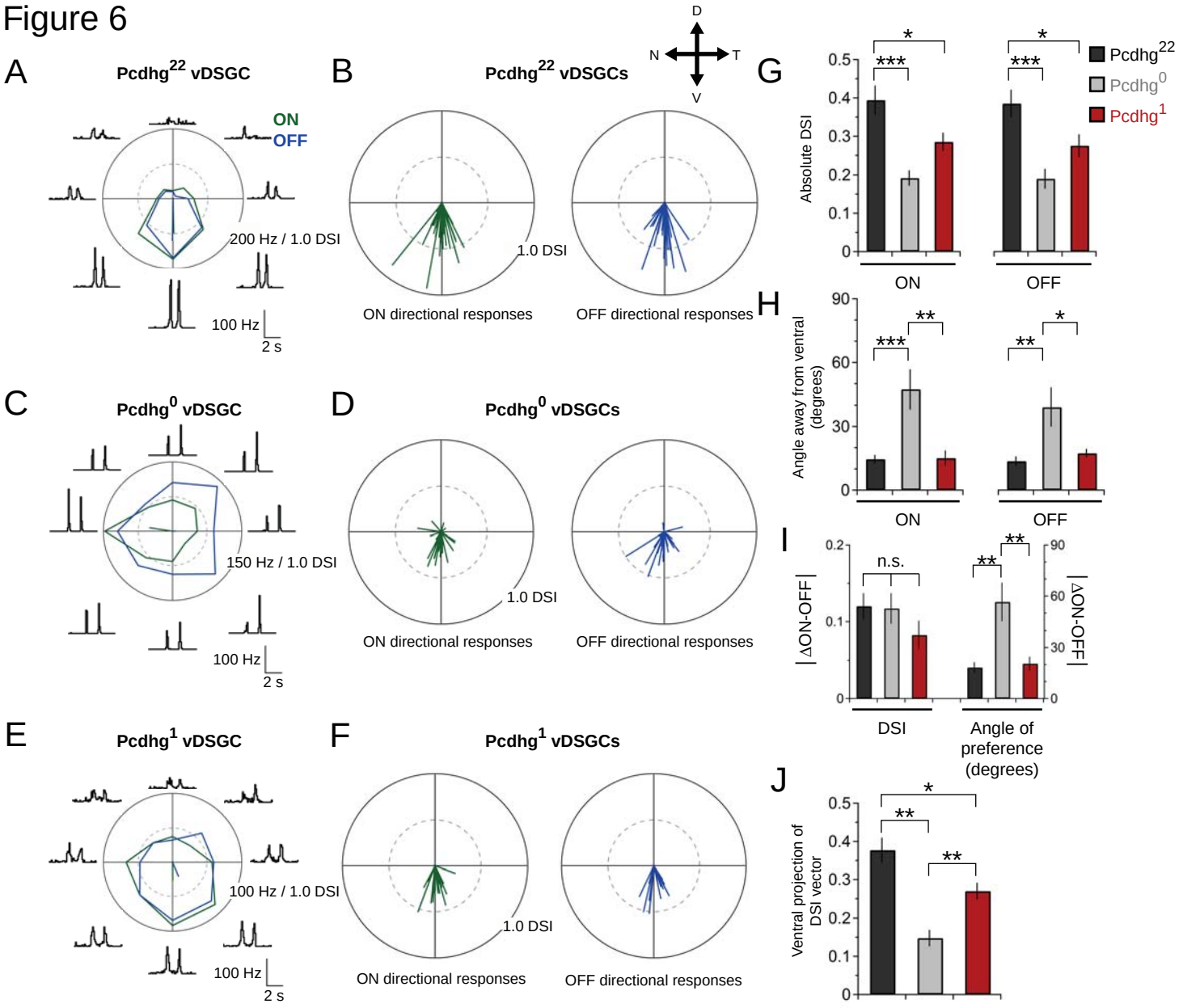
A
Pcdhg22 vDSGC
ON
OFF
200 Hz / 1.0 DSI
100 Hz
2 s
B
Pcdhg22 vDSGCs
D
N
T
V
1.0 DSI
ON directional responses
OFF directional responses
C
Pcdhg0 vDSGC
150 Hz / 1.0 DSI
100 Hz
2 s
D
Pcdhg0 vDSGCs
1.0 DSI
ON directional responses
OFF directional responses
E
Pcdhg1 vDSGC
100 Hz / 1.0 DSI
100 Hz
2 s
F
Pcdhg1 vDSGCs
1.0 DSI
ON directional responses
OFF directional responses
G
Absolute DSI
Pcdhg22
Pcdhg0
Pcdhg1
ON
OFF
H
Angle away from ventral (degrees)
ON
OFF
I
|ΔON-OFF|
n.s.
|ΔON-OFF|
DSI
Angle of preference (degrees)
J
Ventral projection of DSI vector

Figure 7

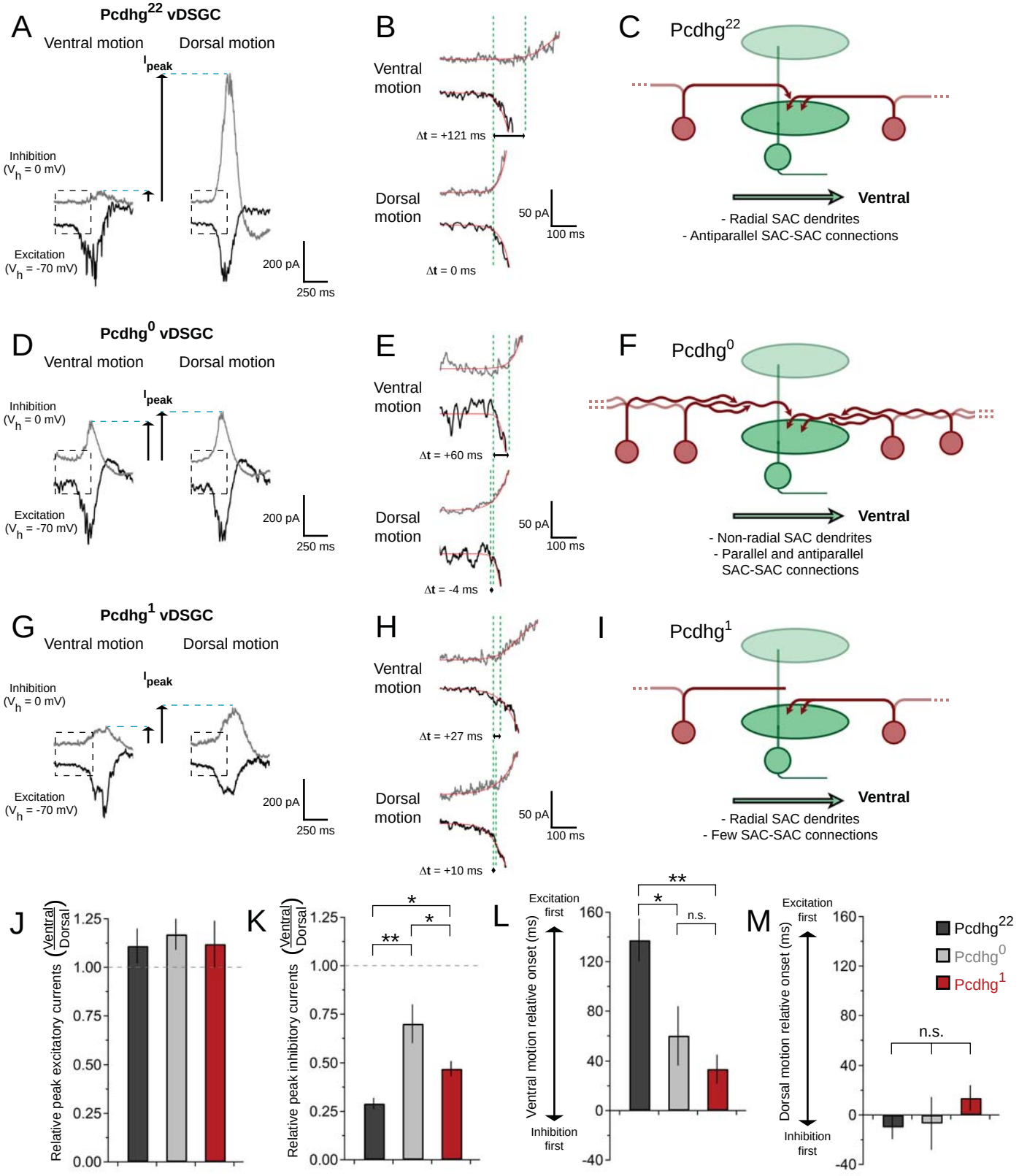
A
Pcdhg22 vDSGC
Ventral motion
Dorsal motion
Ipeak
Inhibition (Vh = 0 mV)
Excitation (Vh = -70 mV)
200 pA
250 ms
B
Ventral motion
Δt = +121 ms
Dorsal motion
Δt = 0 ms
50 pA
100 ms
C
Pcdhg22
Ventral
- Radial SAC dendrites
- Antiparallel SAC-SAC connections
D
Pcdhg0 vDSGC
Ventral motion
Dorsal motion
Ipeak
Inhibition (Vh = 0 mV)
Excitation (Vh = -70 mV)
200 pA
250 ms
E
Ventral motion
Δt = +60 ms
Dorsal motion
Δt = -4 ms
50 pA
100 ms
F
Pcdhg0
Ventral
- Non-radial SAC dendrites
- Parallel and antiparallel SAC-SAC connections
G
Pcdhg1 vDSGC
Ventral motion
Dorsal motion
Ipeak
Inhibition (Vh = 0 mV)
Excitation (Vh = -70 mV)
200 pA
250 ms
H
Ventral motion
Δt = +27 ms
Dorsal motion
Δt = +10 ms
50 pA
100 ms
I
Pcdhg1
Ventral
- Radial SAC dendrites
- Few SAC-SAC connections
J
(Ventral/Dorsal)
Relative peak excitatory currents
1.25
1.00
0.75
0.50
0.25
0.00
K
(Ventral/Dorsal)
Relative peak inhibitory currents
*
*
**
1.25
1.00
0.75
0.50
0.25
0.00
L
Excitation first
Inhibition first
Ventral motion relative onset (ms)
**
*
n.s.
160
120
80
40
0
-40
M
Excitation first
Inhibition first
Dorsal motion relative onset (ms)
Pcdhg22
Pcdhg0
Pcdhg1
n.s.
160
120
80
40
0
-40